USDA Forest Service
U.S. DEPARTMENT OF AGRICULTURE
Rocky Mountain Research Station
RMRS-GTR-444
March 2025

Pollutant Emission Factors for Smoldering Conifer Forest Duff

Shawn P. Urbanski, Shannon Kay, Stephen P. Baker, Emily N.Lincoln, Andrew A. Ross, David Blunck

Urbanski, Shawn P.; Kay, Shannon; Baker, Stephen P.; Lincoln, Emily N.; Ross, Andrew A.; Blunck, David. 2024. **Pollutant emission factors for smoldering conifer forest duff**. Gen. Tech. Rep. RMRS-GTR-444. Fort Collins, CO: U.S. Department of Agriculture, Forest Service, Rocky Mountain Research Station. 45 p.
https://doi.org/10.2737/RMRS-GTR-444

Abstract

Prescribed fires can be a significant source of air pollution with negative consequences for public health and safety. Therefore, smoke management is a key element in the planning and execution of prescribed fires. Emission factors (EF), which quantify the relative abundance of pollutants released by wildland fires, are a needed input for the emission calculations which are essential to effective smoke management. A key challenge when conducting prescribed fires near sensitive receptors such as roadways, communities, and outdoor recreational sites is limiting smoke production from long-term smoldering of coarse dead wood and duff. We carried out a laboratory study to address a knowledge gap in duff EF. We report the EF of carbon dioxide (CO_2), carbon monoxide (CO), methane (CH_4), the sum of 19 nonmethane hydrocarbons (NMHC) and fine particulate matter ($PM_{2.5}$) for smoldering duff during laboratory burns of duff harvested from Douglas-fir forest stands in eastern Oregon. This study suggests the default $EFPM_{2.5}$ used in the First Order Fire Effects Model, a widely used tool for planning prescribed fires and estimating emissions, may significantly underestimate $PM_{2.5}$ emissions for smoldering duff in Western conifer forests.

Keywords: smoke management, prescribed fire, emissions, air quality, smoke impacts, emission factors, smoldering combustion, organic soil

Authors

Shawn Urbanski, Research Physical Scientist, U.S. Department of Agriculture, Forest Service, Rocky Mountain Research Station, Fire, Fuel, and Smoke Research Program, Missoula, Montana

Shannon Kay, Statistician, U.S. Department of Agriculture, Forest Service, Rocky Mountain Research Station Fort Collins, Colorado

Stephen P. Baker, Chemist, U.S. Department of Agriculture, Forest Service, Rocky Mountain Research Station, Fire, Fuel, and Smoke Research Program, Missoula, MT

Emily N. Lincoln, Physical Scientist, U.S. Department of Agriculture, Forest Service, Rocky Mountain Research Station, Fire, Fuel, and Smoke Research Program, Missoula, MT

Andrew Ross, Graduate Student, Oregon State University, College of Engineering, School of Mechanical, Industrial, and Manufacturing Engineering, Corvallis, Oregon

David Blunck, Professor, Oregon State University, College of Engineering, School of Mechanical, Industrial, and Manufacturing Engineering, Corvallis, Oregon

Acknowledgments

This research was funded by the Department of Defense Strategic Environmental Research and Development Program (SERDP), project RC-2651, under contract no. W912HQ-16-C-0045 and USDA Forest Service Research & Development. Technical contributions from and insightful conversations with Daniel Cowan and Benjamin Smucker are gratefully acknowledged.

Contents

This page intentionally left blank.

1. Introduction

Smoke from wildland fires (wildfires and prescribed fires) is a major source of air pollutants (Urbanski et al. 2022). Fine particulate matter (particulate matter with a nominal mean aerodynamic diameter ≤ 2.5 μm; $PM_{2.5}$) is the primary pollutant of concern in smoke due to its deleterious health effects (Jaffe et al. 2020; Reid et al. 2016; USEPA 2019, 2021a) and impacts on visibility (Ashley et al. 2015; Bartolome et al. 2019; National Wildfire Coordinating Group 2020a). In addition to $PM_{2.5}$, fresh smoke contains hundreds of gaseous pollutants, including a wide variety of volatile organic compounds (VOC) capable of producing ozone (O_3) (Alvarado et al. 2015; Jaffe and Widger 2012; Lindaas et al. 2017), a secondary air pollutant, which can have negative impacts on public health and the environment (Grulke and Heath 2020; USEPA 2020; Wittig et al. 2009).

In the United States (U.S.) wildland fire smoke has emerged as a major contributor to poor air quality. Over the past decade, wildfire smoke from both the U.S. and Canada, has been responsible for hundreds of days of unhealthy air quality that has impacted tens of millions of people across the western and central U.S. (Buchholz et al. 2022; Childs et al. 2022; David et al. 2021; O'Dell et al. 2019). Increases in wildfire activity have offset reductions in anthropogenic air pollutant emissions resulting in a long-term trend of worsening air quality in regions prone to wildfire smoke impacts (McClure and Jaffe 2018; O'Dell et al. 2019). In the eastern U.S., large wildfires and major smoke intrusions from distant wildfires (e.g., in the western U.S. or Canada) are infrequent compared with the West (the 11 contiguous western States) (Brey et al. 2018). However, in the central and southeastern U.S., prescribed fire use is widespread (Jaffe et al. 2020; Melvin 2018). According to the 2017 National Emission Inventory (USEPA 2021b), prescribed fires accounted for 31 percent of total $PM_{2.5}$ emissions in the Southeast and were the dominant major emission sector being 80 percent greater than dust and 133 percent greater than fuel combustion, the second and third largest sources.

A prescribed fire is a planned fire conducted to meet land management objectives. Prescribed fires, which are conducted under a set of weather and ecosystem conditions (a prescription), maximize the likelihood the land management objectives will be safely achieved. A primary use of prescribed fire is the mitigation of wildfire hazard through the reduction of fuels (combustible live and dead vegetation), and the restoration and maintenance of ecosystem health (Agee and Skinner 2005). The increased occurrence of large wildfires (> 200 ha) over recent decades (Holden et al. 2018; Westerling 2016), the growth of the wildland-urban interface, and the prospect of more frequent large, high severity wildfires in the future (Abatzoglou and Williams 2016; Kitzberger et al. 2007; Littell et al. 2009; USDA 2014; Westerling et al. 2016) has led to increased interest in prescribed fire as a forest management tool (Ager et al. 2014; Stephens et al. 2021). The U.S. Department of Agriculture, Forest Service, Wildfire Crisis Strategy (WCS) Implementation Plan (USDA 2022) calls for an unprecedented increase in fuels treatments—prescribed fire and mechanical treatments such as thinning and mastication of understory vegetation (Agee and Skinner 2005; Mitchell and Smidt 2019)—across all lands with a focus on the western U.S. In the West, the implementation plan recommends treating up to an additional 20.2 million ha (50 million acres) on

Federal, State, Tribal, and private lands over a period of 10 years succeeded by a long-term treatment plan for maintenance. Successful execution of the implementation plan will require overcoming many challenges, including improving current smoke management capabilities.

Achieving the major expansion of prescribed fire use advocated by the WCS will require providing land managers with improved data, tools, and techniques to minimize the impacts of increased smoke emissions. Concerns regarding smoke management are among the top obstacles to prescribed burning (Melvin 2018). Smoke from prescribed fires can have significant detrimental effects on public health and transportation. Prescribed fires can subject local communities and sensitive populations to unhealthy levels of $PM_{2.5}$. Prescribed fire smoke can also endanger public safety by reducing visibility on roadways, leading to fatal traffic accidents (Ashley et al. 2015; Bartolome et al. 2019). Moreover, since prescribed fires are treated as a controllable emission source the resultant smoke can lead to a regulatory violation of the National Ambient Air Quality Standards (USEPA 2021a).

The impact of wildland fire smoke on specific locations is influenced by the mass of pollutants released (i.e., emissions), how the emissions are lofted into the atmosphere, and the subsequent transport and dispersion of the plume. Emissions are an essential input to smoke forecasting models used to simulate the transport and dispersion of smoke in the atmosphere and the resultant surface concentrations of $PM_{2.5}$ and other harmful pollutants (Urbanski et al. 2022). Estimating emissions is an element of proper smoke management practices as defined in the National Wildfire Coordinating Group Smoke Management Guide for Prescribed Fire (National Wildfire Coordinating Group 2020b). Emissions of a particular pollutant (X) are calculated as the product of the mass of fuel consumed and the emission factor for X, EFX, which is the mass of X produced per mass of fuel consumed by fire (e.g., 20 g of $PM_{2.5}$ per kg of fuel consumed). Emission factors (EF) are influenced by many factors, including fire behavior and fuel properties, that affect combustion, such as the size, shape, packing, and condition of the vegetation to be burned, moisture content, and growth stage (Urbanski et al. 2022). For a given wildland vegetation type, the EF can differ substantially across the various components that may be present, such as tree canopy, grass, shrubs, litter, fine dead wood, coarse dead wood, duff, and duff/peat (Urbanski et al. 2022). Duff and peat, which are moderately to highly decomposed organic materials that make up the Oi, Oe, and Oa soil horizons (Soil Survey Staff. 2022. Keys to Soil Taxonomy, 13th ed. USDA Natural Resources Conservation Service)—below the litter layer (fresh to slightly decomposed twigs, needles, and leaves).

A challenge of managing prescribed fires in forests near sensitive receptors such as roadways, communities, and outdoor recreational sites is limiting smoke production from long-term smoldering of coarse dead wood and duff/peat. The primary combustion phases in wildland fire are flaming and smoldering. Flaming (gas phase) combustion occurs when fuels are heated sufficiently to produce high-temperature volatiles in an oxidative environment. For flaming combustion to occur, there must be sufficient energy delivered to the fuel and resulting volatiles to sustain gas-phase oxidation. As a result, this combustion is typically considered hotter than smoldering-dominated fires.

During flaming phase combustion, nearly all the volatiles (gases, tars, and particulates) are converted to carbon dioxide (CO_2), and the EF for non-CO_2 carbon containing products are relatively small. Litter, fine woody debris (down dead wood with diameter <7.62 cm), shrubs, herbs, and tree crowns are consumed primarily by flaming combustion (Ottmar 2014).

Smoldering (solid phase) combustion occurs at moderate to high temperatures when sufficiently heated solid fuels are converted to char in an oxidative environment. The energy necessary to sustain smoldering combustion is lower than that necessary to sustain flaming combustion. Smoldering combustion typically produces a suite of complex volatiles (gases, tars, and particulates) which, when not paired with flaming combustion, results in a very inefficient combustion process. In smoldering-dominated scenarios, the EF for $PM_{2.5}$, carbon monoxide (CO), and other incomplete combustion products are typically much higher than those for flaming-dominated combustion. Because sustained smoldering combustion requires less energy, there is often less heat produced to drive buoyant plume rise, resulting in smoke plumes closer to the ground (Liu et al. 2022). Conversely, heat released during flaming-dominated combustion is much higher than smoldering alone, providing sufficient energy to loft buoyant smoke plumes further up into the atmosphere.

In wildland fires, much of the coarse dead wood consumption, and nearly all duff/peat consumption, occurs by smoldering (National Wildfire Coordinating Group 2020b; Ottmar 2014). Smoldering of coarse dead wood and duff/peat can continue for hours and even days after the initial passing of the flaming front (Rein 2016). This extended duration smoldering of coarse dead wood and duff/peat is often referred to as residual smoldering. Because smoke from smoldering tends to remain near the surface, the $PM_{2.5}$ and other pollutants emitted often pose a much greater risk to nearby communities and valued resources than emissions lofted into the atmosphere in the buoyant plume of a flame-dominated fire. This is especially true when smoldering persists into the nighttime when the formation of the stable nocturnal boundary layer inhibits vertical mixing, and emissions are trapped in a shallow layer (a few hundred meters) near the surface (Liu et al. 2022). Further, under certain conditions differences in terrain can result in pooling of smoke in low-lying areas (Liu et al. 2022). In complex terrain, this is exemplified by cold drainage flows down a canyon (see for example Miller et al. 2019). However, even in areas with mild local terrain, smoke can accumulate in low lying areas.

The complex terrain of the western U.S. is composed of diverse forest and rangeland ecosystems. Conifer forests cover 82.3 million ha across the western U.S., with pinyon/juniper, Douglas-fir, fir/spruce/mountain hemlock, and ponderosa pine FIA forest type groups accounting for 26 percent, 25 percent, 18 percent, and 14 percent of this forest area, respectively (Ruefenacht et al. 2008; available at https://data.fs.usda.gov/geodata/rastergateway/forest_type/). These forest types are prevalent in the 21 Western priority landscapes selected for priority treatment under the WCS implementation (USDA 2022; 2023). For example, Douglas-fir and ponderosa pine FIA forest type groups account for nearly 50 percent of the total forest area within these landscapes. Duff is an important

component of fuel in these forests, comprising 30–45 percent of total surface and ground fuel loading (Urbanski et al. 2018).

As discussed above, emissions from smoldering duff present special smoke management challenges for prescribed fire use. One of these challenges emerges in the initial stages of smoke management during the calculation of emissions—uncertainty in EF for $PM_{2.5}$ and other pollutants. The EF available in the literature (Akagi et al. 2011; Andreae 2019; Urbanski 2014), served by EF databases (for example, the Smoke Emission Reference Application; Prichard et al. 2020), and used in popular smoke management tools (such as the First Order Fire Effects Model; Lutes 2020), are based primarily on studies of smoldering peat.

Peat and duff are both classified as organic soil material, however the environments in which they are formed differs significantly. Peat is formed in wetlands under anerobic water saturated conditions. Published studies of peat EF for $PM_{2.5}$ ($EFPM_{2.5}$) are based on peat from Alaska (Bertschi et al. 2003; Chakrabarty et al. 2016; Watson et al. 2019; Yokelson et al. 2013), Siberia (Chakrabarty et al. 2016; Watson et al. 2019), coastal North Carolina (Black et al. 2016; Geron and Hays 2013), Florida (Bhattarai et al. 2018; Watson et al. 2019), Malaysia (Bhattarai et al. 2018; Watson et al. 2019), and Indonesia (Christian et al. 2003; Jayarathne et al. 2018; Kuwata et al. 2018; Roulston et al. 2018; Wooster et al. 2018; Yokelson et al. 2022). In contrast, the duff of most western U.S. forests is formed in comparatively dry, upland environments. Given the very different formation environments and the different vegetation inputs, the chemical and physical properties that affect the smoldering behavior, and hence pollutant emissions, may differ considerably between peat and duff.

To support land managers wanting to expand the use of prescribed fire treatments across the West, we conducted a laboratory study to address this knowledge gap in duff EF. Additionally, we investigated the relationship between EF and smoldering temperature. The primary goal of this study was to provide EF data to improve the performance of wildland fire pollutant emission models when applied to the prescribed burning of conifer forests in the western U.S. A secondary study goal was to identify a pollutant emission–smoldering temperature linkage that would support the incorporation of pollutant emissions into models of smoldering (for example Cowan et al. 2020). In pursuit of these goals, we measured the EF for the following: (1) CO_2, (2) CO, (3) methane (CH_4), (4) 19 non-methane hydrocarbons (NMHC), (5) $PM_{2.5}$, and (6) the surface temperatures of smoldering duff during laboratory burns of duff harvested from Douglas-fir forest stands in the McDonald Research Forest in eastern Oregon, U.S.A. In this report we describe the details of the study's methods and measured EF. While we did observe an EF dependence on smoldering temperature due to artifacts associated with our emission sampling method, this EF–T relationship cannot be applied beyond our study. Finally, we conclude by discussing the implications of the EF measured in our study for smoke management in Western conifer forests.

2. Materials and Methods

2.1 Duff Sample Collection and Characterization

Eight laboratory burns were conducted using Douglas-fir duff from the McDonald Research Forest near Corvallis, Oregon, U.S.A. The location and dates of harvest for the duff samples are provided in table 1. The duff samples were collected between two to eight weeks prior to the burns. The samples were collected utilizing a metal extraction jig that was placed 2 m from Douglas-fir trees following the approach reported previously (Cowan et al. 2020). The extraction jig had sharpened metal sides that penetrated through the duff and the soil beneath minimizing disturbances to the duff being extracted. Once the extraction jig was secured in the ground, the duff was isolated from the sides by hammering stainless steel plates around the duff sample. Once isolated from the sides, the duff sample was removed exposing a relatively undisturbed sample 46 cm x 46 cm in area and 3–5 cm thick. A stainless-steel metal sheet was then placed underneath the duff sample isolating it from the ground allowing the entire duff sample to be carefully slid into a cardboard box. Individual samples within the boxes were stored in the laboratory prior to the burns.

In the weeks prior to the burns the moisture content of the duff samples was measured. The moisture content was determined by measuring the mass of a duff subsample prior to and after placing the sample into an oven at 105 °C for a minimum of 48 hours, as outlined in ASTM D2974-87 Method B (ASTM International 2014). If the moisture content of a duff subsample exceeded 80 percent, the parent duff sample was placed in an oven at a temperature of 105 °C to reduce the moisture content. This maximum moisture threshold was selected because in previous studies (Cowan et al. 2020) it was rare for duff samples with a moisture content of greater than 80 percent to ignite and/or have sustained smoldering. The duff sample was removed from the oven after approximately 12 hours and moisture content was measured. The process was repeated until the moisture content of the duff was below the 80 percent threshold.

Prior to being burned, the moisture content and duff thickness were measured using subsamples collected from the corners of the duff. The subsamples were collected using a 5 cm cylinder inserted into the corners of the duff and stored in sealed plastic containers. Additional duff subsamples were sent to an outside laboratory (University of Idaho Analytical Services Laboratory, Moscow, Idaho, U.S.A.) for determination of the carbon content. The outside laboratory determined the duff carbon content by combustion analysis using a LECO CN 628 (LECO Instruments, St. Joseph, MI, U.S.A.). The properties and sample locations of duff burned in this study are provided in table 1.

Table 1A—May dates and conditions of burns and properties and harvest location of duff samples burned.

Burn	Burn date	Percentage of duff moisture content	Duff depth (cm)	Bulk density (kg m^{-3})	Percentage of carbon content	Outdoor air temperature[a,b] (C)	Percentage outdoor relative humidity[a,b]	Number of emission samples	Duff collection date	Duff collection location
1	5/12/2021	13.2	3.18	44.8	49.5	— (18.7)	— (49.9)	7	4/29/2021	44.63990, –123.28392
2	5/12/2021	40.8	3.81	74.4	48.7	— (23.4)	— (36.2)	14	4/29/2021	44.63990, –123.28392
3	5/13/2021	7.0	4.57	71.4	49.9	— (20.7)	— (52.3)	11	4/19/2021	44.63754, –123.29185
4	5/13/2021	9.3	3.02	128.1	49.1	— (23.0)	— (46.6)	13	4/19/2021	44.63754, –123.29185

Table 1B—January dates and conditions of burns and properties and harvest location of duff samples burned.

Burn	Burn date	Percentage of duff moisture content	Duff depth (cm)	Bulk density (kg m^{-3})	Percentage of carbon content	Outdoor air temperature[a,b] (C)	Percentage outdoor relative humidity[a,b]	Number of emission samples	Duff collection date	Duff collection location
1	1/28/2020	19.7	—	—	31.4	9.2 (9.0)	86 (87)	7	12/3/2019	44.63991, –123.30571
2	1/29/2020	17.0	—	—	43.1	8.8 (9.7)	88 (77)	9	12/3/2019	44.63991, –123.30571
3	1/30/2020	5.8	—	—	33.5	8.0 (9.1)	95 (85)	6	1/15/2020	44.64104, –123.31060
4	1/31/2020	13.1	—	—	43.8	14.8 (16.0)	83 (71)	15	1/15/2020	44.64104, –123.31060

— indicates a blank cell.

[a] Source: Outdoor ambient air temperature and relative humidity data obtained from the MesoWest weather and climate archive (https://mesowest.utah.edu/) Horel et al. (2002).

[b] First value is data from the Corvallis Municipal Airport KCVO (latitude 44.5000, longitude -123.2833, elevation 75 m, distance from OSU campus 7 km) and value in parentheses is from Eugene Mahlon Sweet Field KEUG (latitude 44.1333, longitude -123.2144, elevation 111 m, distance from OSU campus 42 km). Meteorological station KCVO did not report data on May 12 and 13 of 2021.

2.2 Experimental Approach

Smoldering experiments were conducted at Oregon State University in Corvallis, Oregon, U.S.A. The test building was an insulated, but unheated shed. During emissions testing, the shed was ventilated with outdoor air entering through an open garage door and exiting through a ventilation fan in the shed's ceiling. Air temperature (T_{air}) and relative humidity (RH) within the shed approximated outdoor conditions during testing. The experimental arrangement is shown in figure 1. The experimental arrangement included a coflow, an infrared (IR) camera, and a stainless-steel mirror. The IR camera was used to capture images of the smoldering to later determine surface temperatures, the area of active smoldering, and fire radiative power. The stainless-steel mirror was used to reflect the IR images from the smoldering reaction, protecting the IR camera from smoke and minimizing smoke obscuration of the camera's view. The experimental arrangement was enclosed by a series of fire-resistant curtains, protecting the experiment from external disturbances (i.e., air currents).

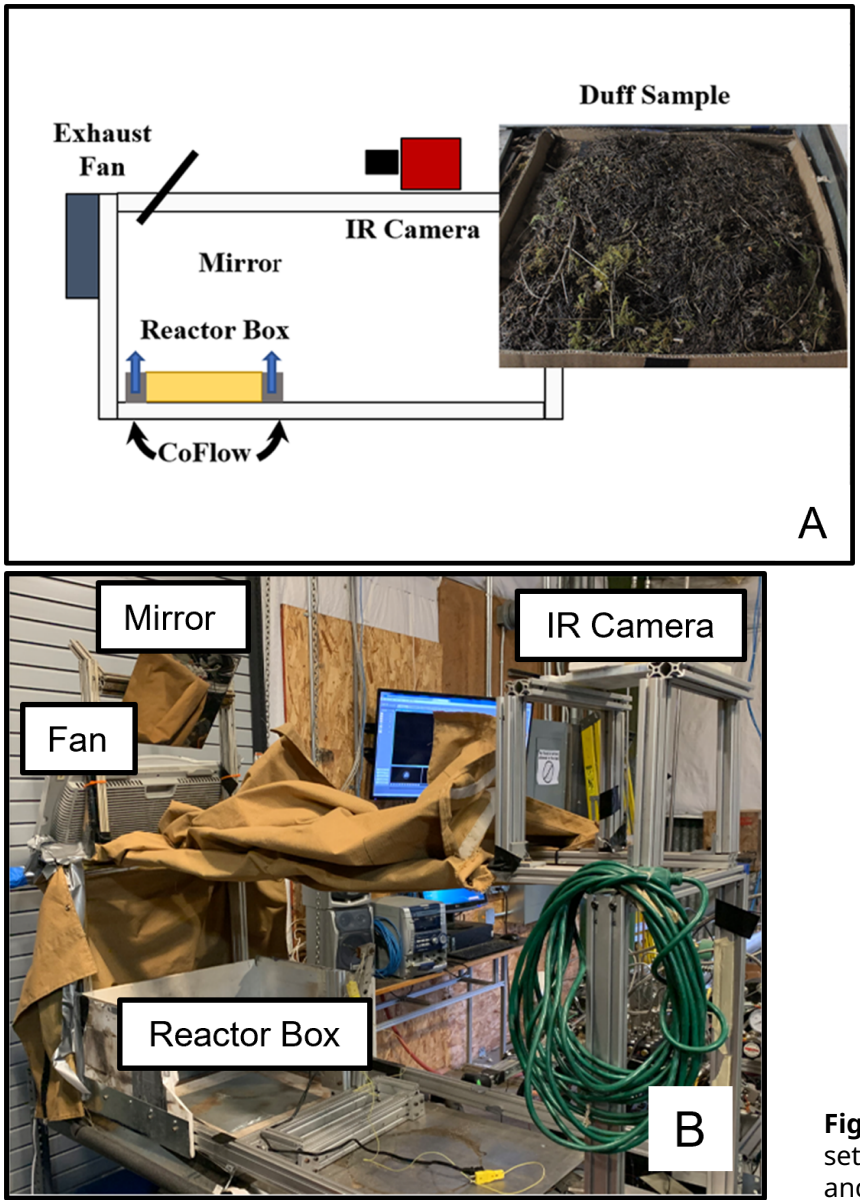

Figure 1—Diagram of emissions testing setup and duff sample prior to testing (A) and photo of emissions testing setup (B).

The IR camera used was a FLIR SC6700 (FLIR Systems, Inc., Oregon, U.S.A.) with a spectral range of 3.0–5.0 μm. An integration time of 4.96 ms was utilized, which corresponds to a temperature range of 80 °C to 730 °C, which was within the bounds of previous smoldering experiments (Cowan et al. 2020). The IR camera was set to capture images every 10 seconds. The window of the IR camera was set to 640 x 512 pixels. A spatial calibration image was taken prior to each burn utilizing a heated plate. The spatial resolution varied slightly between experiments but was typically 0.62 mm pixel^{-1}.

The coflow was used to reduce the inter-test variation in local T_{air} and RH during cold conditions (i.e., < 14 °C). The coflow provided a heated, low velocity sheath of air (< 0.2 m s^{-1}) upward around the reactor box, along all four edges of the sample and not through the samples. The air supplied to the coflow was dried air from a building compressor. In previous work (Cowan et al. 2020), it was estimated that the coflow controlled local T_{air} and RH above the samples to mean values of 14 °C (±5 °C) and 51 percent (±11 percent) (values in parenthesis one stand deviation), respectively; however, T_{air} and RH above the duff samples were not monitored in this study. At the time of testing, laboratory T_{air} ranged from an estimated 7 °C to 24 °C, and the samples were at the laboratory T_{air} prior to testing. When testing occurred at T_{air} >14 °C the coflow apparatus was used to provide consistency between burns, but the air was not heated beyond 14 °C.

The approximate dimensions of the duff samples burned were 43 cm x 43 cm x 4 cm, although some natural variation occurred. The duff samples were kept in cardboard boxes during the burns. Prior to burning, the cardboard boxes were cut flush with the top of the duff samples. Stainless-steel plates were placed under and around the duff sample to reduce the risk of cardboard burning.

Duff ignition was achieved using a 1500 W heat gun with an exit diameter of 2.5 cm, following the approach reported in Cowan et al. (2020). The heat gun was set and preheated at its highest temperature and lowest fan speed setting. Upon sufficient preheating (roughly 2 minutes), the heat gun was placed at the center of the duff sample within 5 cm of the duff surface. The heat gun was applied until flames were observed. Once flames were observed, the heater was removed and the flames were quenched by smothering with a fire-resistant glove. The ignition method created a circular shaped area of smoldering duff which was allowed to propagate freely.

The smoldering burn was monitored utilizing the IR camera to ensure smoldering persisted. If the IR camera indicated that the smoldering reaction had peak photon counts below 2,200 (corresponding to about 230 °C, see section 2.3) and there was no visible smoke being emitted, ignition was reattempted using the aforementioned procedure. If ignition was unsuccessful after two hours, the samples were considered unable to support self-sustained smoldering and the test was aborted. Once ignition was successfully achieved, self-sustained smoldering samples were monitored visually and using the IR camera. Transition from smoldering to flaming was observed on multiple occasions and when flames were observed they were quenched utilizing a fire-resistant glove. The experiment was concluded once the smoldering front reached the edge

of the reactor box. Duration of the smoldering experiments ranged from 0.5 to 4.3 h. Periodically throughout the burns, emissions samples were collected (section 2.4).

2.3 Analysis of Infrared Camera Data

The IR images were used to determine surface temperatures (T; °C), smoldering area (A; cm^2), irradiance (I; W m^{-2}), and fire radiative power (FRP; W). Image processing was conducted utilizing R Statistical Software (v4.1.2; R Core Team 2021) and the R package ijtiff (v2.2.7; Nolan and Padilla-Parra 2018). The photon counts provided by the IR camera were converted to temperatures utilizing a blackbody calibration performed previously (Cowan et al. 2020). The calibration used blackbody temperatures that ranged from 100 °C to 550 °C and an integration time of 4.96 ms and is described in Appendix A.

The A, T, I, and FRP of actively smoldering regions were determined from the IR camera images for the interpretation and modeling of pollutant emissions. For each image, pixel level photon counts were converted to T using the blackbody calibration (Appendix A). Then pixels were separated into two groups: smoldering and non-smoldering. Pixels with T > 180 °C were considered smoldering. We selected the threshold of 180 °C based on numerous studies of duff and peat pyrolysis and combustion, which have found that organic components begin to decompose and generate volatiles in the temperature range of 160 °C–200 °C (Chen et al. 2011; Chen et al. 2013; Huang and Rein 2016; Yang et al. 2016; Zhao et al. 2014; Zhu and Lui 2020).

The total A, mean T, and total FRP of actively smoldering regions were calculated on a per image (camera frame) basis, using only pixels classified as smoldering (T > 180 °C; 453.15 K). For each actively smoldering pixel k, I (W m^{-2}) was determined with equation 1:

$$I_k = \sigma \varepsilon T_k^4 \tag{1}$$

where σ is the Stefan Boltzmann constant (5.67037 x 10^{-8} W m^{-2} K^{-4}), ε is the estimated emissivity of the duff (0.85; Lopez et al. 2013), and T_k is the pixel temperature (K) determined from the pixel photon count and blackbody calibration. Within an image, *i*, the fire radiative power, FRP_i, was calculated using equation 2, where I_{bkgd} is the background irradiance contribution for each pixel, A_i is the area of active smoldering in the image (m^2), which is calculated with equation 3 wherein n_k is the number of smoldering pixels and A_{pixel} is the pixel area (0.3844 mm^{-2}). The I_{bkgd} was calculated from equation 1 with T_k = 453.15 K (180 °C), the threshold for smoldering.

$$FRP_i = A_i \sum_{k=1}^{n_k} (I_k - I_{bkgd}) \tag{2}$$

$$A_i = n_k A_{pixel} \tag{3}$$

Six image averages of A and T were used for the analysis of the emissions data to approximate the typical emission sampling duration of about 60 s (section 2.4). The images were cropped and analyzed to only include pixels that were covered by the emission sampling chamber (section 2.4). Thus, the reported values of A, T, and FRP correspond directly to the region where emissions were being sampled. Presample and postsample quantities from the IR camera were calculated from six-image blocks immediately before and immediately after each emission sample. The pre- and postsample quantities were used to identify perturbations to smoldering by the emission sampling method (section 3.2).

2.4 Emission Sampling

Emissions were collected as a series of gas and filter samples that began after smoldering commenced. Samples were taken at approximately 10–20 minute intervals depending on visible smoke activity and the IR image. The emissions sampling was accomplished by placing a small, open-faced cubic chamber (0.027 m^3) onto the smoldering duff (Appendix B, fig. B.1). The chamber had a footprint of 0.09 m^2 (30 cm x 30 cm), with a small, battery-operated fan inside the top to gently mix the smoke. There were two ports at the top of the chamber, one for gas samples and one for particulate filter samples. For the particulate filters, 1 m of non-static tubing connected one port to the filter sampling unit, and the other port used a 1 m length 0.635 cm (0.25 in) inside diameter Bev-A-Line® tubing to the gas canister sampling unit.

The canister sampling unit consisted of a 12-volt swing piston pump (model UNPK09DC, 12 L $minute^{-1}$ maximum flow rate, KNF, Trenton, NJ) plumbed with stainless steel tubing, a pressure relief valve and pressure gauge. The canisters were 850 ml stainless steel, with an electropolished inner surface, and a 0.25 in NUPRO stainless steel bellows sealed valve (model SS-4H1-NN). Prior to use, the canisters were evacuated and cleaned per United States Environmental Protection Agency methods TO-14A (USEPA 1999). Canister gas samples were drawn from the chamber and pressurized to approximately 20 psia over 30 s.

The filter sampling system consisted of a custom apparatus designed and assembled in-house, consisting of a pump (Thomas model SR-0300), flow controllers and control electronics, and a URG model 2000-30EH 2.5 µm cut point Teflon coated aluminum cyclone, with a flow rate of 16.7 Lpm. The filters were Teflon (Pall Corp.) 1 µm pore size, 37 mm diameter. The sampling pump was calibrated with a Gilibrator-2 air flow calibrator device (Sensidyne, LP, Florida, U.S.A.). Flow rate and time of sampling were logged to determine sample volume. Images of the filter sampling system are provided in Appendix B, figure B.2.

Periodically, during the burn experiments, a background canister sample was collected to establish the initial concentration (i.e., the background) of gases without smoldering emissions. To sample smoldering emissions, the chamber was placed onto the area of actively smoldering duff and smoke was allowed to fill the chamber. The duration of time that the chamber filled varied from 30 to 60 s. Fifteen seconds prior to the chamber fill duration time, gas canister and particulate filter sampling was initiated. Canister sampling lasted 30 s, starting 15 s prior to the chamber fill duration, to achieve

an average concentration for the chamber fill period. The filter sampling time varied, depending upon how quickly the filter loaded and the air flow decreased; usually, the filter sample took less time than for the canister sample. The chamber was then removed allowing the duff to smolder unperturbed until the next emission sample.

2.5 Analysis of Emission Samples

The canisters were analyzed at the Forest Service Missoula Fire Sciences Laboratory (Missoula, MT, U.S.A.). The concentrations (in units of parts per million by volume, ppm) of CO_2, CO, CH_4, and 19 NMHC (Appendix C, table C.1) were determined by gas chromatography following Environmental Protection Agency method TO-14A (USEPA 1999) with an Agilent model 7890 gas chromatograph (Santa Clara, CA, U.S.A.) equipped with dual flame ionization detectors (FID). Each FID has a specific column, 10-port valve in a heated zone, gas sampling loop, and plumbing setup. Agilent Open Lab software was used to control the instrument and collect data.

Analyses for CH_4 and NMHC were performed using a 0.25 ml sample loop, a 5 m HP-1 precolumn, a 0.53 mm x 30 m Al/S (Agilent) column, helium carrier gas at 6 ml min^{-1}, and FID at 300 °C, with a makeup helium gas flow of 14 ml min^{-1}. The sample was injected onto the pre-column, then at 1 min, a 10-port valve vented the sample flow coming from the precolumn to exhaust, to prevent heavier hydrocarbons going through the main column and on to the detector.

The CO_2 and CO analysis used a 10-port valve with a 1 ml sample loop to inject the sample, a 0.3175 cm (1/8 in) diameter x 1.829 m (6 ft) Carbosphere (Alltech; Deerfield, IL U.S.A.) column to separate CO_2, CO, and air, helium carrier gas at a flow rate of 16 ml min^{-1}. After separation in the column, the sample enters a nickel catalyst methanizer (375 °C), that converts the CO_2 and CO to CH_4, then on to a flame ionization detector (FID), temperature 350 °C. The column was back flushed at 15 min, after elution of the CO_2 peak. The two analyses (CO/CO_2, hydrocarbons) were run simultaneously with an oven temperature program of 50 °C for 6 min, then increasing by 10 °C min^{-1} to a final temperature of 150 °C for 8 min.

Chromatogram data was processed by Agilent Open Lab software. A set of gas standards bracketing the sample concentrations were analyzed with each set of samples to construct a standard curve for each compound. Based on the integrated peak areas, the sample concentrations were calculated from the standard curves and entered into a Microsoft Excel spreadsheet. Duplicate analyses were performed every sixth sample. The National Institute of Standards and Technology primary standards were analyzed to verify the accuracy of the standards.

The 37 mm Teflon filters were conditioned and weighed in a controlled-environment room at 20 °C and 35 percent RH. Prior to weighing, the filters were conditioned for at least 24 h. Each filter was weighed three times on a Mettler M4 microbalance (Mettler–Toledo; Columbus, OH U.S.A.) with a precision of 1 µg. The balance was linked to a software program that collects and stores the weights and room conditions. The balance was tared (zeroed) before each weighing. A calibration weight was used once every five filters to verify the accuracy and calibration of the microbalance. Filters whose weights

were not reproducible to within 5 μg are withheld from use in sampling. Control filters were used to correct for environmental and handling variability in the filter weights. The control filters were handled in the same way as the treatment filters. Each filter was preweighed prior to sample collection using this procedure, and then again after field collection. When returned with particulate samples the filters were again conditioned at least 24 h to stabilize the particulate matter weights and to reduce the effects of static electricity on the weighing process.

2.6 Emissions Calculations

Pollutant emissions in the smoke samples were quantified using the excess mixing ratio, which for species X is defined as $\Delta X = X_{smoke} - X_{background,}$ where X_{smoke} and $X_{background}$ are the mixing ratio of X in fresh smoke and background air, respectively. Analysis of the canister samples (section 2.5) provided volume mixing ratios which were converted to mass mixing ratio (mg m^{-3}) at standard conditions of temperature (298 K) and pressure (1 atmosphere). Mass mixing ratios of $PM_{2.5}$ were calculated from the filter particulate matter weights (postweight minus preweight), control filter results, and the volume of air drawn through the filter during the emission sampling. The carbon mass balance method (USEPA 2022; Ward and Radke 1993) was used to calculate the EF for each species X, EFX (X-g fuel-kg^{-1}; where fuel is the dry mass of biomass burned) for each sample using equation 4:

$$EFX = 1000 F_c \frac{\Delta X}{\Delta C_T} \quad (4)$$

In equation 4, ΔC_T is the sum of the excess mass mixing ratios of carbon in all measured species (CO_2, CO, CH_4, 19 NMHC, and $PM_{2.5}$), F_c is the mass fraction of carbon in the dry biomass (table 1), and the factor 1000 provides EF units as g kg^{-1}. We assumed the carbon mass fraction of $PM_{2.5}$ was 0.70 (Burling et al. 2011; Watson et al. 2019). The carbon mass balance method assumes all biomass carbon that is volatilized as gases and particulate matter is measured and included in the denominator of equation 4 (see Urbanski 2014). Fresh biomass smoke contains hundreds of organic gases; however, even though our study measured carbon in just 23 species (CO_2, CO, CH_4, 19 NMHC, and $PM_{2.5}$), this results in only minor overestimates as most of the carbon (>90 percent) in biomass smoke is contained in CO_2, CO, and CH_4 (Urbanski 2014). Our emission measurements were also used to calculate modified combustion efficiency ($MCE = \Delta CO_2 / (\Delta CO_2 + \Delta CO)$) an index for the relative amount of flaming and smoldering (Yokelson et al. 1999). In a completely efficient combustion process, 100 percent of the biomass carbon would be converted to CO_2 (MCE = 1.0). For pure smoldering (the absence of flame), MCE ≤ 0.85 (Akagi et al. 2011).

3. Results and Discussion

3.1 Summary of Burns

Emission measurements were obtained from burns of eight duff samples conducted in January 2020 and May 2021 at the Oregon State University testing facility. During the laboratory burns, 79 emission samples with coincident IR camera data were collected and analyzed. The burns are summarized in table 1. The emission samples were used to calculate ΔX and calculate EF for 22 carbonaceous gases (CO_2, CO, CH_4, and 19 NMHC) and $PM_{2.5}$, as described in section 2.6. During burn 1 of the May 2021 tests, a significant flame-up occurred, and following quenching of the flames, we were unable to achieve consistent smoldering. Two emission samples were collected during this post-flame-up period, but they have not been included in our analysis. Additionally, for the last two emission samples of burn 4 in May 2021, $PM_{2.5}$ measurements were not obtained due to a malfunction of the filter sampling system. These two samples have also been excluded from our emissions analysis. Thus, for the May 2021 tests, only 40 emission samples were analyzed.

The ambient conditions of the burns and their possible impact on the combustion process must be considered when assessing and utilizing these data. The test facility's ventilation system drew in exterior air to remove exhaust, and the T_{air} and RH within the testing facility were similar to the outdoor environment. A coflow was operated to condition T_{air} and RH around the duff sample (section 2.2) and previous work (Cowan et al. 2020) estimated the coflow controlled local T_{air} and RH to mean values of 14 °C (±5 °C) and 51 percent (±11 percent) (values in parenthesis are one standard deviation). However, T_{air} and RH above the duff samples were not monitored in this study, which raises concerns regarding the January tests. The ambient RH during the January testing exceeded 80 percent (table 1), which is very atypical of prescribed burn conditions. Understory broadcast prescribed burns of the type we aimed to emulate in this study are usually conducted in spring or fall with the reduction of dead surface fuels, such as litter and fine woody debris, being a primary objective. The flammability and combustion completeness of these dead fuels depends highly on their moisture content, which tracks ambient RH (National Wildfire Coordinating Group 2020b; Prichard et al. 2022). It is highly unlikely an understory prescribed burn would be attempted under the ambient RH of our January testing. Therefore, if the coflow failed to appreciably reduce the RH of the ambient air, our January tests will be an unreasonable proxy for estimating duff emissions from prescribed burns. Lacking measurements of T_{air} and RH around the duff samples during testing, we elected to evaluate the combustion behavior using FRP derived from the IR camera data (section 2.3).

Studies on the combustion of wildland fuels have found that the mass of fuel consumed is correlated with fire radiative energy (FRE, J), the time integral of FRP (Freeborn et al. 2008; Wooster et al. 2005). As a proxy for fuel consumption, we estimated dry biomass emitted (*EDM*; g), by applying the fuel carbon fraction (table 1) to total carbon emitted:

$$EDM = vol \frac{\Delta C_T}{F_c} \quad (5)$$

where ΔC_T and F_C are as defined in (equation 4) and vol is the volume of the sample chamber (0.027 m^3). The FRE was calculated as the product of FRP and the sample duration, which ranged from 30 to 60 s. For this analysis we used the average of the pre- and post-sample FRP. Figure 2 plots EDM versus FRE for the January and May tests. The May burns were consistent with previous studies, EDM was highly correlated with FRE (r = 0.82, p-value = 1.5e-11). However, EDM was not correlated with FRE for the January burns (r = -0.03, p-value = 0.85). These findings indicate the two sets of burns had very different burning behavior with that of the January burns departing significantly from that reported in previous studies. Therefore, the analysis and presentation of results is limited to the May burns, which were conducted under ambient conditions typical of prescribed burns and exhibited combustion behavior consistent with previous studies. The emission measurements of the January burns are summarized in Appendix D to provide complete reporting of the study. However, given the peculiar combustion behavior of the January burns and the possibility that ambient conditions were not representative of broadcast prescribed burns in the western U.S., we highly discourage use of these data for estimating pollutant emissions. *Apart from Appendix D, the remainder of this report is limited to the May tests.*

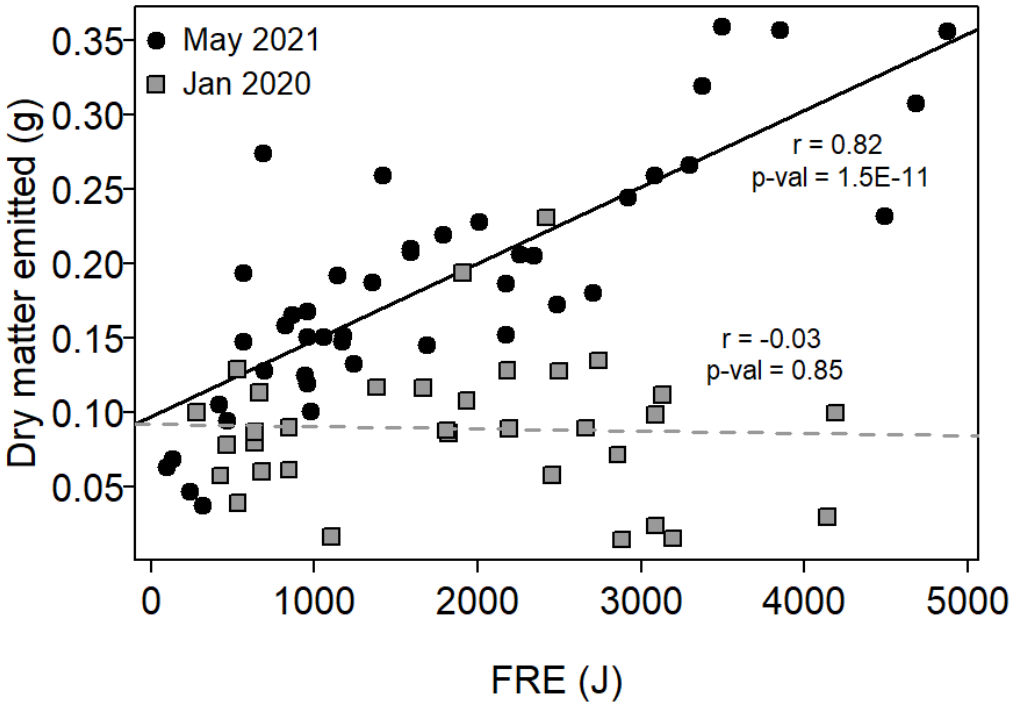

Figure 2—Dry matter emitted plotted versus FRE. Solid black line and dashed gray line are best fit linear regression models to May and January data, respectively.

3.2 Smoldering Perturbation

The emission sampling method, which involved gently placing an open-faced cubic chamber over the duff surface (section 2.4), tended to perturb the smoldering. Figure 3 shows IR camera frames immediately before and after an emission sample and figure 3(a), the area of actively smoldering pixels (T>180 °C; white), is visibly reduced after sampling. For the emission sample depicted in figure 3, the change in A was -17.0 cm^2 (from 219.0 cm^2 to 202 cm^2) and the average T of the smoldering pixels decreased

1.1 °C (from 260.2° C to 259.1 °C), based on the six IR camera frames immediately before and after sample collection. To assess the significance of smoldering perturbations associated with the emission sampling, we compared changes in A and T before and after emission sampling with natural variability as outlined in figure 4a. The A and T values were quantified using blocks of six IR camera frames to approximate the typical emission sampling duration of approximately 60 s. Perturbations associated with emission sampling were calculated as:

$$\Delta A = A_{post} - A_{pre} \tag{6a}$$

$$\Delta T = T_{post} - T_{pre} \tag{6b}$$

Natural variability of smoldering was quantified using a six-frame block which ended 60 s prior to each pre-sample block (fig. 4a) to simulate the passage of time during emission sampling:

$$\Delta A_{natural} = A_{pre} - A_{pre\text{-}60} \tag{7a}$$

$$\Delta T_{natural} = T_{pre} - T_{pre\text{-}60} \tag{7b}$$

We compared the six-frame averages of A and T for each of the 40 samples. We found that the emission sampling tended to reduce A and T and that the magnitudes of these reductions were large relative to the natural variability. The distribution of ΔA (equations 6a and 7a) and ΔT (equations 6b and 7b) associated with emissions sampling and natural variation are plotted in figure 4b. The ΔA associated with emissions sampling was negative for 55 percent of samples and the median change was -1.6 percent, compared with 2.2 percent for natural variability. Similarly, the ΔT observed with emissions sampling was skewed negative with a median value of -2.7 °C *versus* -0.1 °C for natural variability. We conclude that the emissions sampling method perturbed the smoldering process with a tendency to reduce A and T. Our approach to account for these perturbations is described in section 3.3.

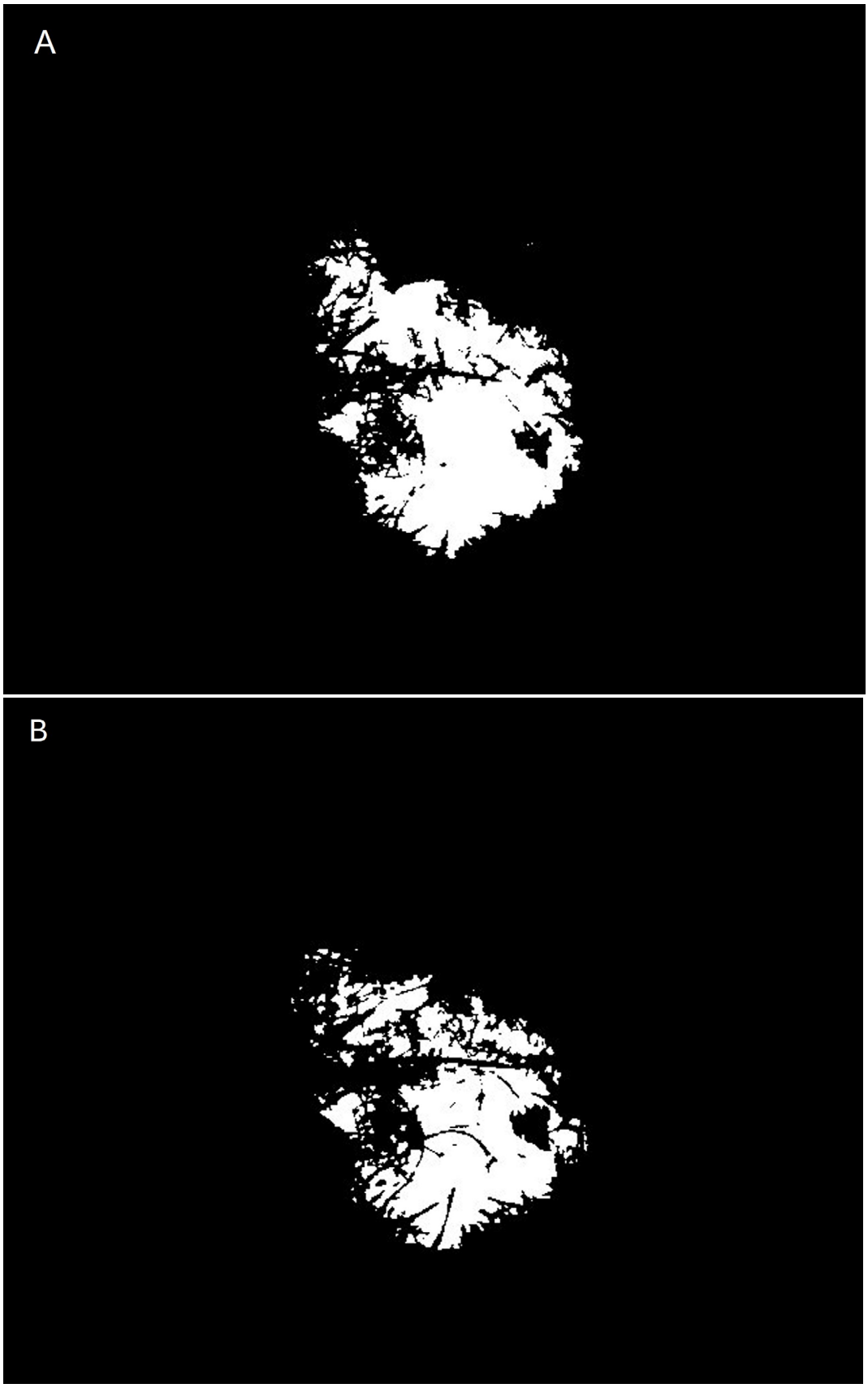

Figure 3—The IR camera image immediately before (A) and after (B) an emission sample. White regions are actively smoldering (T>180 °C). Frame dimensions are 39.68 cm x 31.74 cm.

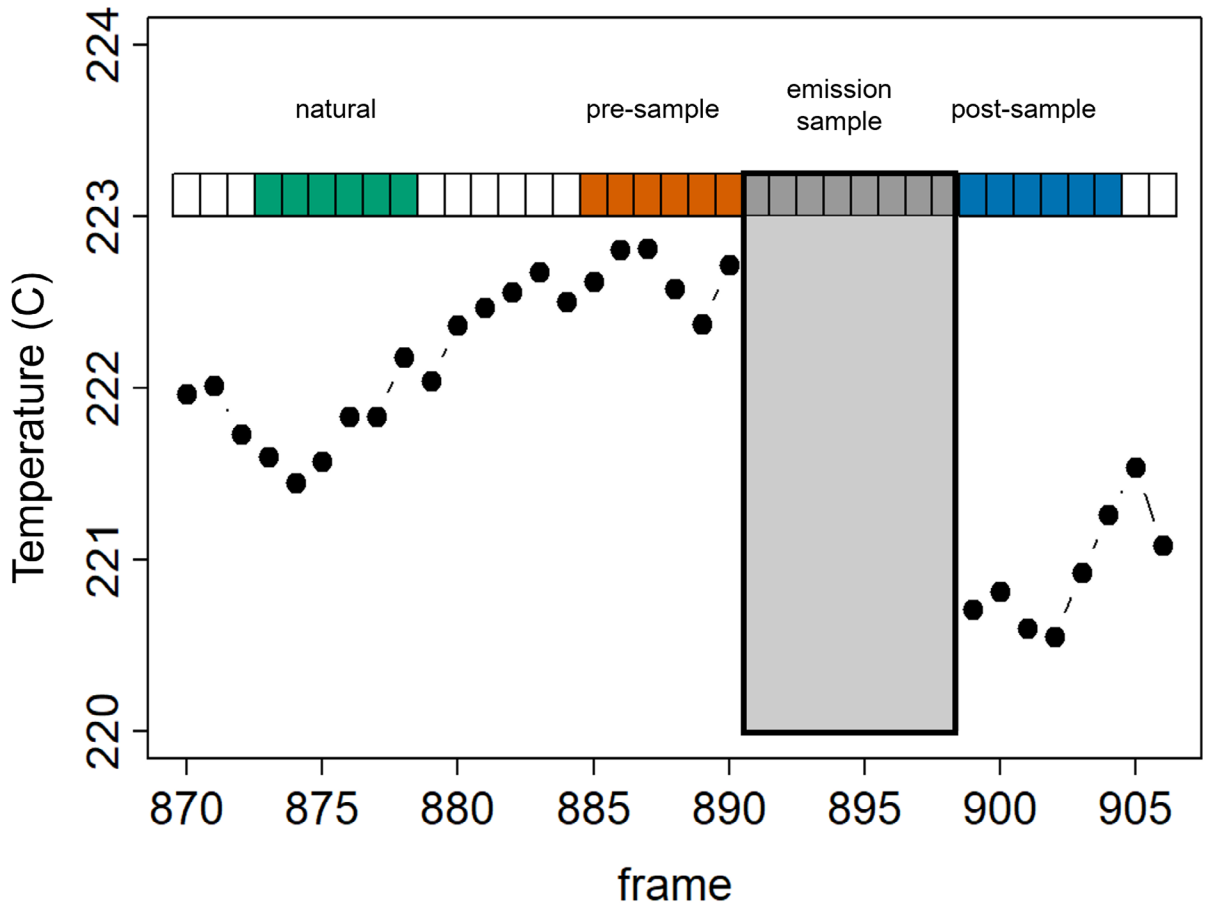

Figure 4a—Surface temperature time series and time position of IR camera frame image blocks used in the perturbation analysis relative to emission sample. The IR camera frame images blocks are 10 seconds.

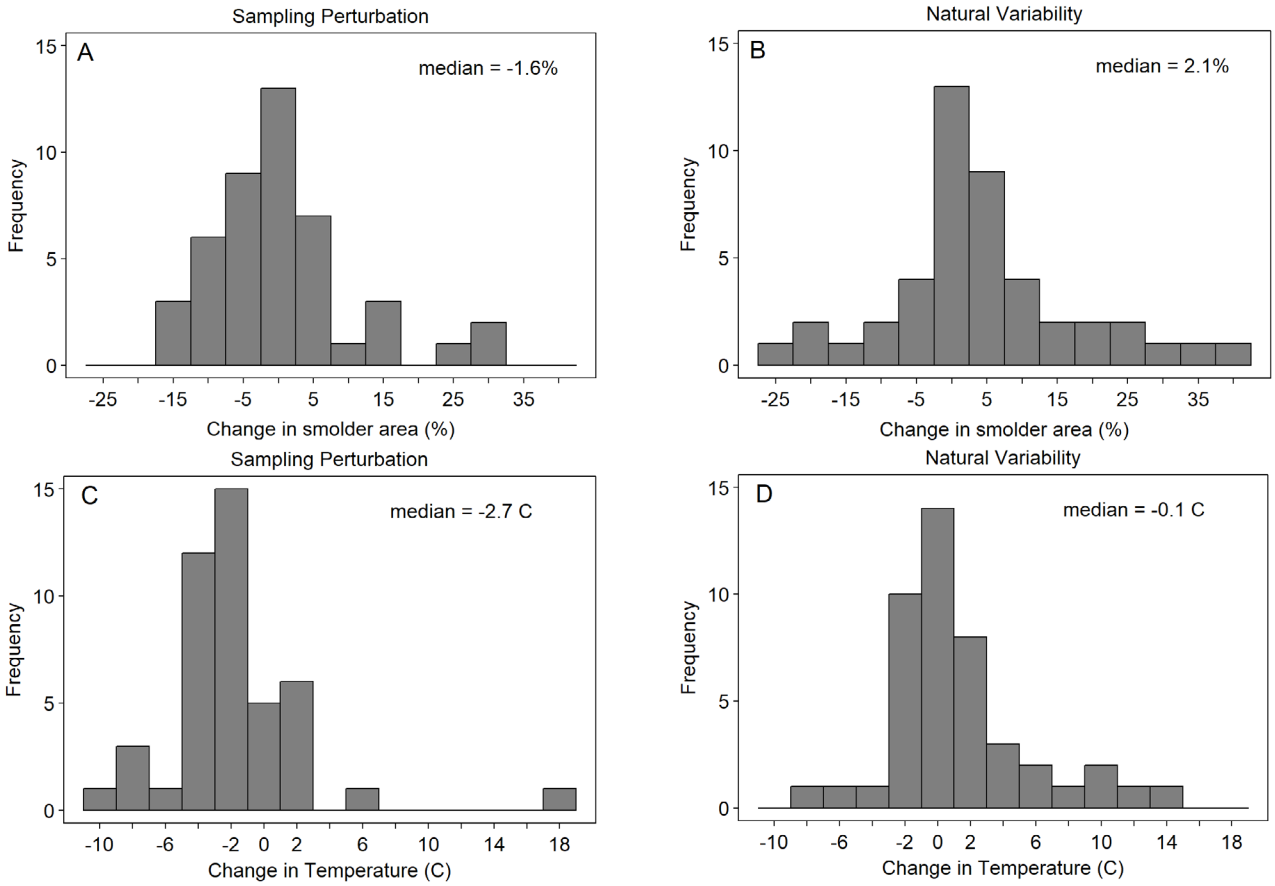

Figure 4b—Frequency distributions of the fluctuations in smoldering area and surface temperature after (A, C) and before (B, D) emissions samples for 40 emission sampling events.

3.3 Emission Factors and Smoldering Perturbation

The emission sampling method perturbed the smoldering process potentially introducing artifacts into our EF measurements. Therefore, we examined the observed EF, EF_{obs}, for dependence on T_{sample} ($T_{sample} = 0.5(T_{pre} + T_{post})$). This undertaking also serves a primary study goal: identify a pollutant emission–smoldering temperature linkage that could support the incorporation of pollutant emissions into models of smoldering. Figure 5 plots the EF_{obs} for CO_2, CO, CH_4, NMHC, and $PM_{2.5}$ versus T_{sample} with the best-fit least square linear regression models and the associated correlation coefficients (r) and p-values (where NMHC is the sum of all 19 hydrocarbons measured, Appendix C, table C.1). In our tests, the EF for CO_2 and CO decrease with increasing T_{sample} while the EF of CH_4, NMHC, and $PM_{2.5}$ show the opposite response (fig. 5). This analysis indicates the emission sampling method not only perturbed the smoldering process, but also introduced artifacts into the observed EF. To account for the effect of the emission sampling (T perturbation) on the observed EF, we chose to use a Bayesian framework to quantify the response of EF to T and derive a best-estimate EF that represents the true EF of the natural, unperturbed smoldering duff.

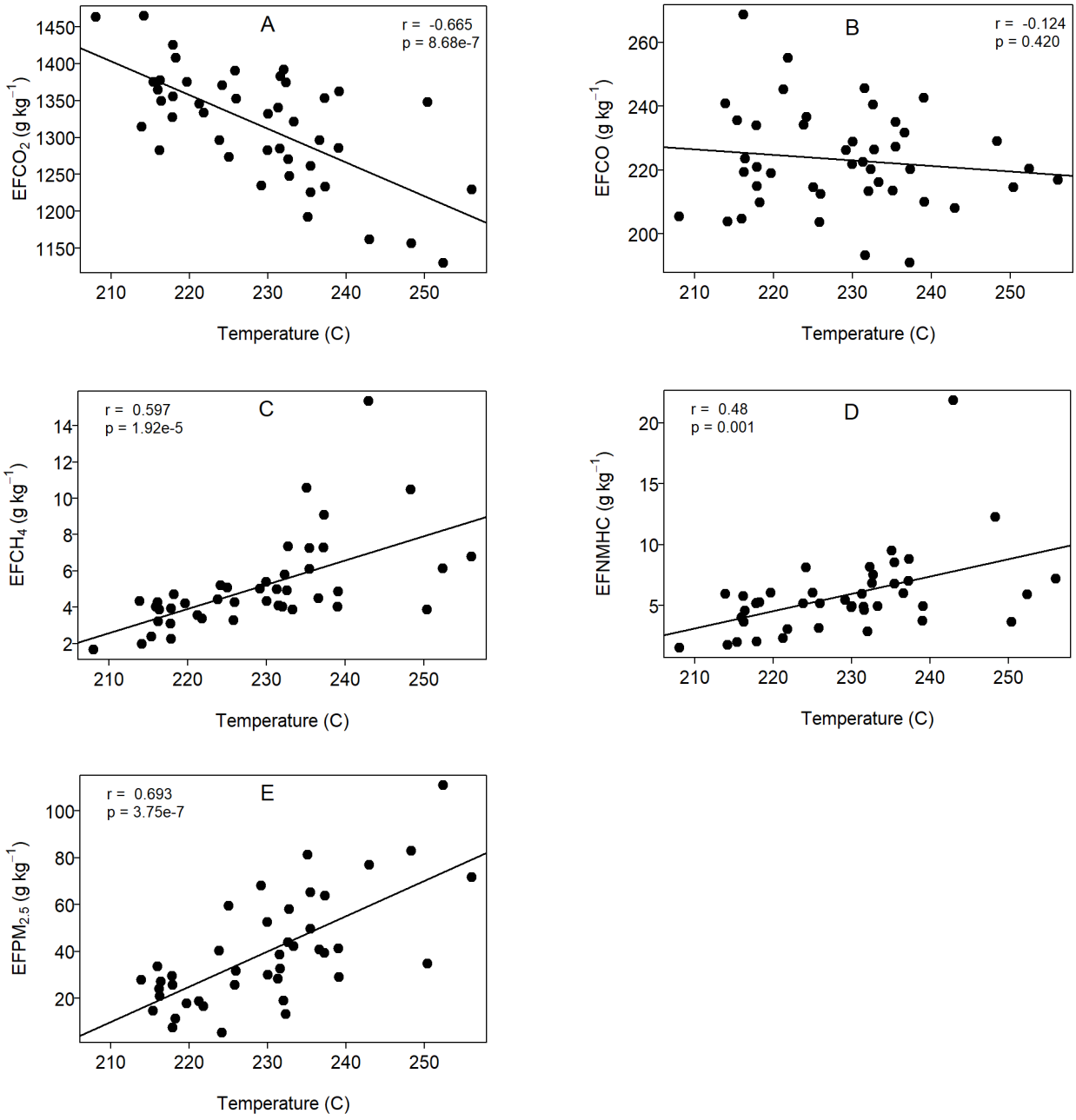

Figure 5—EF_{obs} plotted versus Temperature for CO_2 (A), CO (B), CH_4 (C), NMHC (D) and $PM_{2.5}$ (E) from May testing (table 1) with correlation coefficient (r) and p-value (pval). Solid line is best-fit linear least squares regression model.

The Bayesian framework was used to jointly fit an autoregressive model (AR1) to impute missing T values (T during emission sampling) and a multivariate normal data model to fit five EF responses ($EFCO_2$, EFCO, $EFCH_4$, EFNMHC, and $EFPM_{2.5}$) to the temperature time series. Let $\mathbf{z}_{i,t}$ represent the vector of EF responses for burn *i* at time *t* with shared linear parameters of **α** and **β** across burns relating EF responses to temperature, then the model specification is given by equations 8a–8g:

$$Temp_{i,t} = Temp_{i,t\text{-}1} + \varepsilon \tag{8a}$$

$$\boldsymbol{z}_{i,t} \sim MVN\left(\boldsymbol{\alpha} + \boldsymbol{\beta} Temp_{i,t}, \sum\right) \tag{8b}$$

$$\boldsymbol{\beta} \sim N\left(0, \sigma_{\beta}^{2} \boldsymbol{I}\right) \tag{8c}$$

$$\boldsymbol{\alpha} \sim N\left(0, \sigma_{\alpha}^{2} \boldsymbol{I}\right) \tag{8d}$$

$$Temp_{i,1} \sim Beta\left(1,1\right) \tag{8e}$$

$$\sum^{-1} \sim Wish_{5}\left(\boldsymbol{I}, 6\right) \tag{8f}$$

$$\varepsilon \sim IG\left(1,1\right) \tag{8g}$$

Beta priors were used for the random starts for the first steps in each of the temperature time series, and a global uninformative inverse gamma prior was used for the error term. Independent normal priors with mean zero and variance of one ($\sigma_{\alpha}^{2} = 1, \sigma_{\beta}^{2} = 1$) were used for the shared parameters (**α**, **β**) in the linear predictor function for each response. Initial models to impute temperature included a scalar multiplied by the lag term, $Temp_{i,t} = \theta Temp_{i,t-1} + \epsilon_t$, but θ was estimated to be nearly 1 so it was omitted from the final model.

To aid in model convergence, data were normalized (distributions shifted to [0,1] support) prior to fitting the model and results were back-calculated and shown on the original scale. The Bayesian model was fit using the *jagsUI* package (Kellner 2021) to call JAGS (Plummer 2003) from the statistical software program R (R Core Team 2023). Posterior summaries and model diagnostics were assessed using the MCMCvis package

(Youngflesh 2018). Traceplots were visually assessed and the Gelman-Rubin statistic ("Rhat"; Gelman and Rubin 1992) for each parameter was calculated to evaluate model convergence. Twenty-five thousand iterations were sampled with a burn-in of 2,000 using 3 chains and thinning every fifth iteration. The following packages were also used for data manipulation and graphical displays of results: plyr (Wickham 2011), ggplot2 (Wickham 2016), DescTools (Signorell 2023), ggpubr (Kassambara 2023), and ggpmisc (Aphalo 2024).

3.2 Results of Bayesian Analysis

The posterior reconstruction of time series for T, $EFCO_2$, EFCO, $EFCH_4$, EFNMHC, and $EFPM_{2.5}$ produced with the Bayesian analysis are shown in figure 6 and the optimized model coefficients (**α**, **β**) and credible intervals are provided in table 2. Plots of the EF responses to T for each burn are provided in Appendix E, figure E.1. The model's posterior predicted mean EF account for T perturbations associated with the emission sampling method and are thus taken as the best-estimate EF, which represents the true EF of the natural, unperturbed smoldering duff. From this point forward, EF refers to the best-estimate EF—the Bayesian model posterior predictions of EF. The EF (with 95 percent credible intervals) and EF_{obs} for each burn and the "global" means across all burns are shown in figure 7 and table 3.

Table 2—Bayesian model coefficients (α, β) for EFX = α + βT. Coefficient mean, standard deviation (Stdev), median and 95 percent confidence intervals for X = CO_2, CO, CH_4, NMHC and $PM_{2.5}$.

EFX	Coefficients	Mean	Stdev	2.5%	50%	97.5%	Ř
CO_2	Intercept (α)	0.79	0.11	0.59	0.79	0.99	1
CO_2	Slope (β)	-0.49	0.21	-0.89	-0.49	-0.08	1
CO	Intercept (α)	0.52	0.11	0.32	0.52	0.74	1
CO	Slope (β)	-0.29	0.21	-0.71	-0.28	0.13	1
CH_4	Intercept (α)	0.20	0.10	0.01	0.20	0.40	1
CH_4	Slope (β)	0.45	0.20	0.06	0.45	0.84	1
NMHC	Intercept (α)	0.27	0.10	0.07	0.27	0.48	1
NMHC	Slope (β)	0.33	0.21	-0.1	0.33	0.74	1
$PM_{2.5}$	Intercept (α)	0.12	0.09	-0.05	0.12	0.30	1
$PM_{2.5}$	Slope (β)	0.69	0.18	0.34	0.69	1.04	1

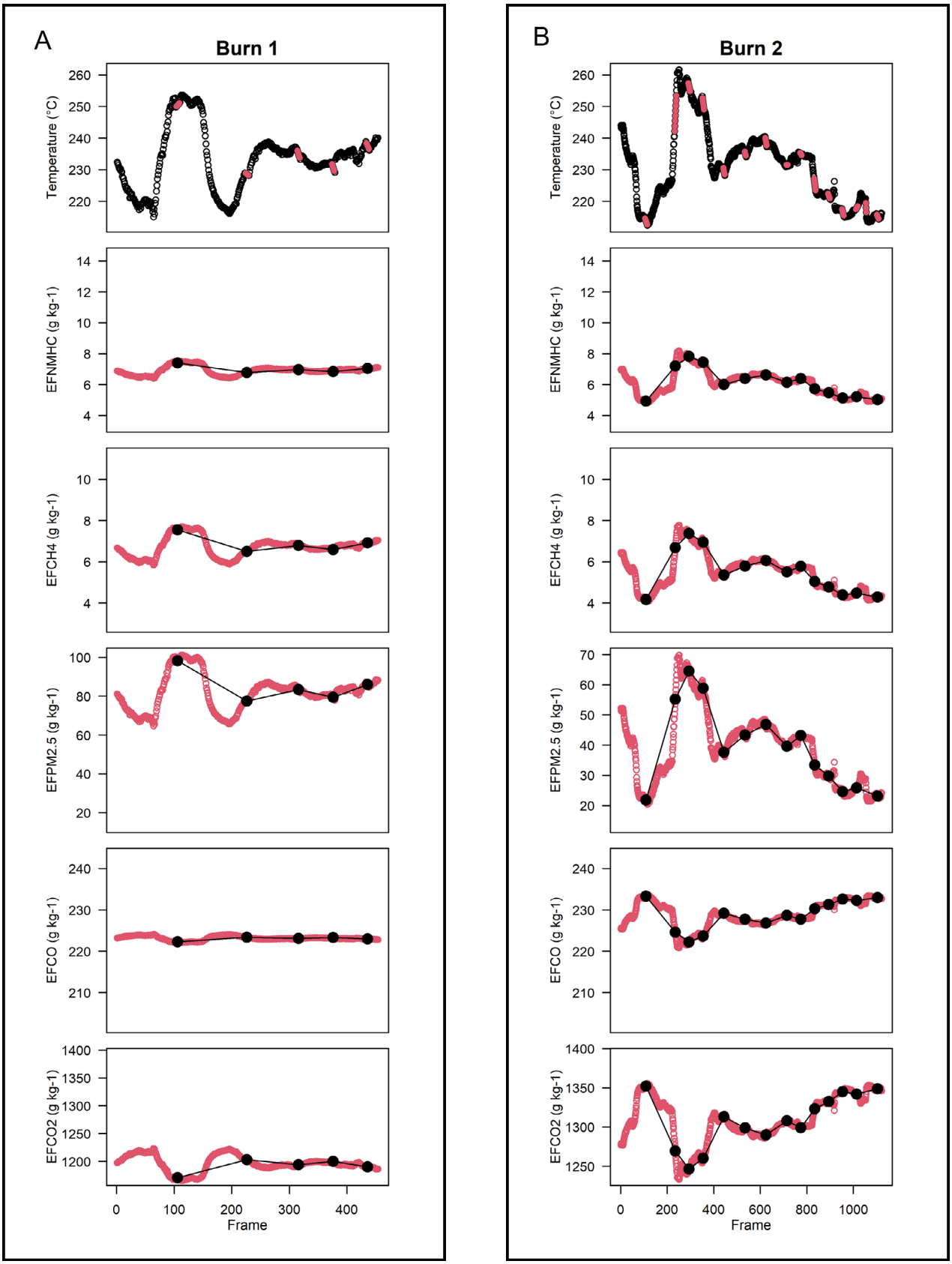

Figure 6A—Posterior reconstruction of time series for T (°C) and EF (g kg^{-1}). T (1st row), EFNMHC (2nd row), $EFCH_4$ (3rd row), $EFPM_{2.5}$ (4th row), EFCO (5th row) and $EFCO_2$ (6th row) for burns 1-2 (A-B). Observed values are shown in black and posterior estimates are shown in pink.

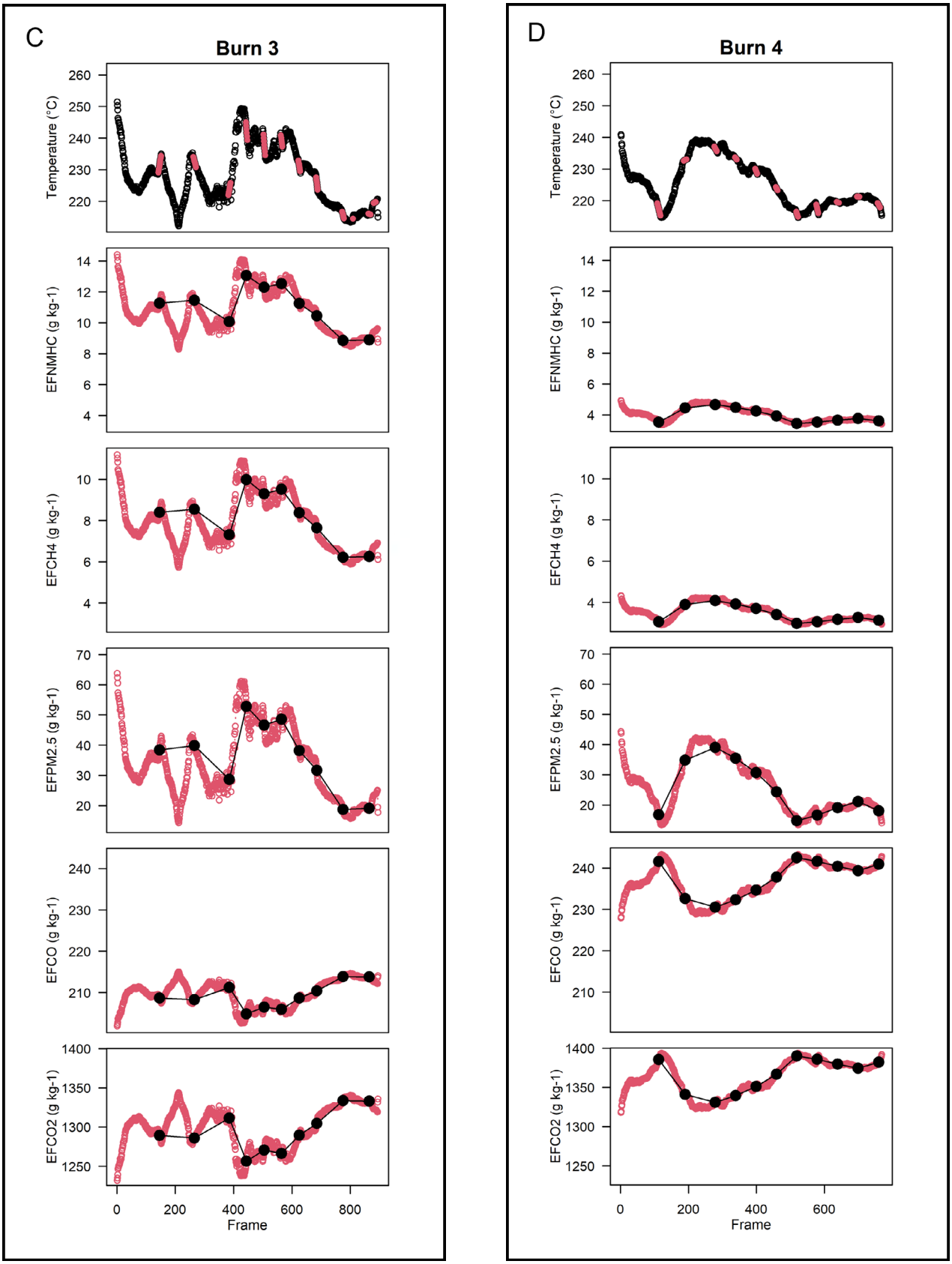

Figure 6B—Posterior reconstruction of time series for T (°C) and EF (g kg^{-1}). T (1st row), EFNMHC (2nd row), $EFCH_4$ (3rd row), $EFPM_{2.5}$ (4th row), EFCO (5th row) and $EFCO_2$ (6th row) for burns 3-4 (C-D). Observed values are shown in black and posterior estimates are shown in pink.

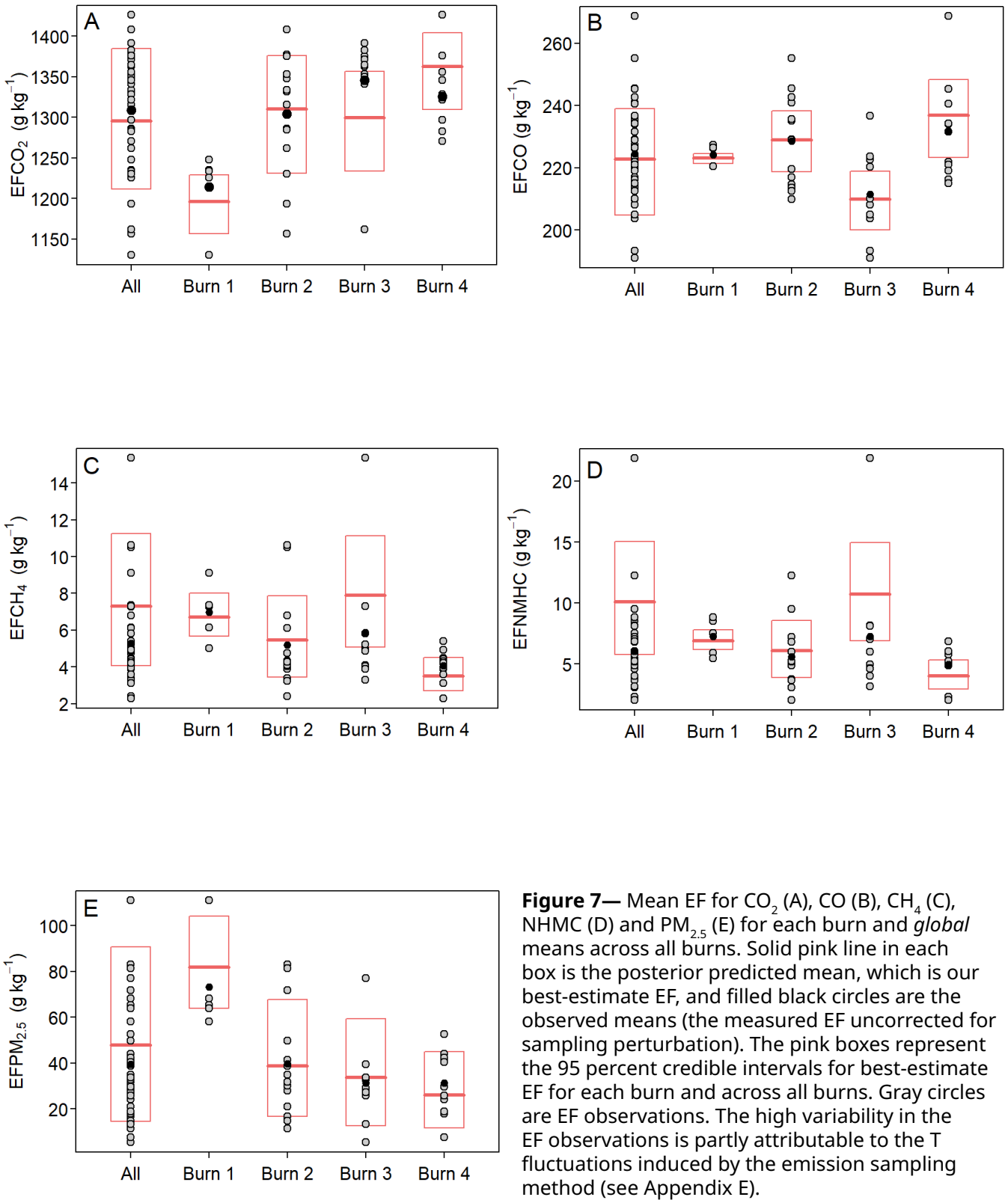

Figure 7— Mean EF for CO_2 (A), CO (B), CH_4 (C), NHMC (D) and $PM_{2.5}$ (E) for each burn and *global* means across all burns. Solid pink line in each box is the posterior predicted mean, which is our best-estimate EF, and filled black circles are the observed means (the measured EF uncorrected for sampling perturbation). The pink boxes represent the 95 percent credible intervals for best-estimate EF for each burn and across all burns. Gray circles are EF observations. The high variability in the EF observations is partly attributable to the T fluctuations induced by the emission sampling method (see Appendix E).

Table 3—Mean EF (g kg^{-1}) and MCE for each burn and "global" means across all burns. Data includes the posterior predicted mean EF and MCE, which is our best-estimate EF and MCE, and the associated 95 percent credible intervals ($CI_{0.025}$ and $CI_{0.975}$) and observed means, the measured EF and MCE uncorrected for sampling perturbation.

Variable	Burn	Mean	$CI_{0.025}$	$CI_{0.975}$	Observed
$EFCO_2$	Burn 1	1196	1156	1229	1214
$EFCO_2$	Burn 2	1310	1231	1376	1304
$EFCO_2$	Burn 3	1300	1234	1357	1346
$EFCO_2$	Burn 4	1363	1310	1404	1326
$EFCO_2$	All burns	1296	1211	1385	1309
EFCO	Burn 1	223	221	225	224
EFCO	Burn 2	229	219	238	229
EFCO	Burn 3	210	200	219	211
EFCO	Burn 4	237	223	248	232
EFCO	All burns	223	205	239	225
$EFCH_4$	Burn 1	6.71	5.65	8.02	6.98
$EFCH_4$	Burn 2	5.45	3.43	7.87	5.20
$EFCH_4$	Burn 3	7.89	5.09	11.13	5.89
$EFCH_4$	Burn 4	3.49	2.70	4.50	4.05
$EFCH_4$	All burns	7.30	4.07	11.23	5.28
EFNMHC	Burn 1	6.92	6.18	7.81	7.27
EFNMHC	Burn 2	6.09	3.87	8.55	5.59
EFNMHC	Burn 3	10.72	6.90	14.94	7.26
EFNMHC	Burn 4	4.01	2.95	5.31	4.96
EFNMHC	All burns	10.08	5.80	15.04	6.05
$EFPM_{2.5}$	Burn 1	81.8	63.8	104.1	73.3
$EFPM_{2.5}$	Burn 2	38.8	16.7	67.8	39.7
$EFPM_{2.5}$	Burn 3	33.8	12.7	59.4	31.3
$EFPM_{2.5}$	Burn 4	26.1	11.7	45.0	31.3
$EFPM_{2.5}$	All burns	47.9	14.6	90.8	39.5
MCE	Burn 1	0.773	0.769	0.777	0.775
MCE	Burn 2	0.785	0.782	0.786	0.784
MCE	Burn 3	0.798	0.797	0.798	0.802
MCE	Burn 4	0.785	0.789	0.783	0.784
MCE	All burns	0.787	0.787	0.790	0.787

The emission samples were collected over a T range of 210–260 °C (figure 6, Appendix E, figure E.1). As T increased over this range, the partitioning of carbon shifted from CO_2 and CO to CH_4, NMHC, and $PM_{2.5}$ (table 2, Appendix E, figure E.1). The $EFPM_{2.5}$ had the strongest response to T with $\beta = 0.69$ g °C^{-1}, while EFCO had the weakest response, $\beta = -0.29$ g °C^{-1}. However, since our emission sampling method perturbed the smoldering process, these EF–T relationships should not be considered applicable beyond our study.

Smoldering involves simultaneous and competing reactions—pyrolysis reactions that decompose the duff producing volatile emissions (gases and particles) and char and the heterogenous oxidation reactions converting char (char oxidation) and unpyrolyzed duff into volatile emissions and ash (Hadden et al. 2013)—which likely yield different emissions. These competing reactions occur over different temperature ranges which vary with duff/peat properties (Cancellieri et al. 2012; Chen at al. 2011; Chen et al. 2013; Palamba et al. 2023; Usup et al. 2004).

Our sampling measured a mixture of emissions produced by these competing reactions. Therefore, the Bayesian model used to correct for the T perturbation caused by the emission sampling method used the average T of all actively smoldering pixels (T >180 °C). While our Bayesian model provides valid estimates and credible intervals for the EF of the unperturbed smoldering duff, it does not allow us to hypothesize the relative contributions of the different smoldering reactions to the emissions produced. Therefore, we are unable to link our EF–T relationships to mechanistic models of duff smoldering. Further, due to the artifacts associated with our emission sampling method, the EF–T relationships cannot be applied beyond our study.

3.4 Summary of Emission Factors

Burn average EF with confidence intervals are given in table 3 and summarized in figure 7. The relative range in burn average EF (maximum EF / minimum EF) was much larger for $PM_{2.5}$ (3.1), NMHC (2.7), and CH_4 (2.3), as compared to CO_2 (1.1) and CO (1.1). For CH_4, NMHC, and $PM_{2.5}$, the lowest average EF were all measured for burn 4 ($EFPM_{2.5}$ for burns 3 and 4 were both 31.3 g kg^{-1}), and the highest were all measured for burn 1. The intraburn spread in EF, as quantified with the coefficient of variation (CV; σ/μ), varied considerably across species. Carbon dioxide and carbon monoxide consistently had an intraburn variability (<0.04) lower than that of CH_4, NMHC, and $PM_{2.5}$ (0.04–0.36). The $EFPM_{2.5}$ had the largest CV for all four burns. Burn average MCE ranged from 0.773 to 0.798 (table 3), which was within the range expected for pure smoldering (Akagi et al. 2011).

3.5 Comparison with Previous Results

With only four burns, we are unable to assess the influence of moisture content or other duff properties (e.g., bulk density or ash content) on EF. Lacking sufficient burns to differentiate emissions by duff characteristics, we have aggregated results from the four burns into study averages (with confidence intervals; table 3) for comparison with previous studies and for assessing the study's potential implications for smoke production from smoldering duff. Our study's best-estimate EF from table 3 is reproduced in table 4 along with results from two previous laboratory studies that

reported the EF for western U.S. conifer forest duff, Selimovic et al. (2018) and Bertschi et al. (2003).

Table 4— Comparison of study average EF (g kg^{-1}) with previous studies. The values in parentheses are 95 percent confidence intervals for our study and standard deviations for the previous studies.

Pollutant	This study[a]	Bertschi et al. (2013)	Selimovic et al. (2018)[b]
MCE	0.789 (0.787, 0.790)	0.865 (0.012)	0.861 (0.030)
CO_2	1296 (1211, 1385)	1464 (13)	1265 (55)
CO	223 (205, 239)	146.0 (15.7)	130.0 (26.8)
CH_4	7.30 (4.07, 11.23)	7.53 (3.25)	10.9 (3.2)
$PM_{2.5}$	47.9 (14.6, 90.8)	9.0 (3.3)	—

— indicates no data.

[a] From table 3.

[b] Calculated from their supplemental material.

There are several published studies of EF for smoldering peat (Black et al. 2016; Hu et al. 2019; Stockwell et al. 2014, 2016; Watson et al. 2019), but we limit our focus to western U.S. conifer duff. Compared with the previous laboratory studies, we measured a lower EF for CH_4 and a higher EFCO, although for $EFCH_4$, all three studies agree within their uncertainty bounds. The major difference is for $EFPM_{2.5}$, which in our study was nearly five times that of Bertschi et al. (2003). The different methods and analyses used in our study and Bertschi et al. (2003) may contribute to large difference in reported $EFPM_{2.5}$. However, the $EFPM_{2.5}$ measured in our study are consistent with the more recent study by Jen et al. (2019). They examined emissions of organic particulate matter for a range of western U.S. wildland fuels, including five burns of coniferous duff. Jen et al. (2019) do not provide EF for individual burns in tabular form; however, careful examination of figure 4a in their article indicates a median EFOC of approximately 30 g kg^{-1} for the coniferous duff burns. Assuming an $EFPM_{2.5}$ to EFOC ratio of 1.4, as observed for smoldering peat (Watson et al. 2019), we estimate an $EFPM_{2.5}$ of 42 g kg^{-1} as a median value for their duff burns, which is in rough agreement with our study's best estimate $EFPM_{2.5}$ of 47.9 g kg^{-1}.

3.6 Emissions and Duff Moisture

In general, increasing the moisture content of wildland fuels such as litter and dead wood tends to increase smoldering, thus reducing MCE and increasing the EF for CO, CH_4, NMHC, oxygenated organic gases, and $PM_{2.5}$ (Urbanski et al. 2022). However, in the natural environment, duff and peat burn predominantly by smoldering (Ottmar 2014; Prichard et al. 2022). While moisture content is an important factor influencing duff/peat ignition and consumption (Cowan et al. 2020; Frandsen 1987, 1997; Ottmar 2014), its influence on EF is unclear. With only four burns, our study cannot test for the effect of moisture content on EF. Previous studies of emissions from smoldering of western U.S. montane conifer duff did not explore the role of moisture content (Bertschi et al. 2003; Selimovic et al. 2018). However, a few studies have explored the effects of moisture content on the EF from smoldering peat, but the findings were

inconsistent. Hu et al. (2019) measured emissions from smoldering premilled Irish peat (initial moisture content of 0, 75, and 160 percent) and found that as moisture content increased, $EFCO_2$ and $EFCH_4$ decreased while EFCO and $EFPM_{2.5}$ increased. In contrast, Watson et al. (2019) reported that increasing the moisture content of Florida peat from approximately 25 percent to approximately 60 percent resulted in reductions of 20 percent for EFCO, 12 percent for $EFCH_4$, 30 percent for $EFPM_{2.5}$, and an increase of 11 percent for $EFCO_2$.

3.7 Implications for Land Management

Estimating emissions is an essential element of proper smoke management practices for prescribed fire (National Wildfire Coordinating Group 2020b). The main goal of our study is the improvement of emission models used for smoke management of prescribed fires. One widely used tool for planning prescribed fires and estimating emissions is the First Order Fire Effects Model (FOFEM; Lutes 2020). The FOFEM is used for calculating the immediate effects of prescribed fire and wildfire on ecosystems: tree mortality, fuel consumption, pollutant emissions, and soil heating. Here we assess the potential impact of our study on FOFEM emission estimates.

We begin by focusing on $PM_{2.5}$, the primary pollutant of concern in wildland fire smoke due to its negative impacts on visibility and health and its regulation as a criteria air pollutant with ambient concentration limits under the Federal National Ambient Air Quality Standards (NAAQS). FOFEM version 6.4 and higher offer two EF options—default and expanded. The FOFEM default value for the $EFPM_{2.5}$ of smoldering duff is 22.6 g kg^{-1}, less than half of our study's best estimate value of 47.9 g kg^{-1} (table 3). The FOFEM default values for $EFPM_{2.5}$, $EFCO_2$, EFCO, and $EFCH_4$, are based on an EF–MCE linear regression model developed from emissions measurements of prescribed fires in chaparral (Ward and Hardy 1989) and logging slash (Ward et al. 1989). The FOFEM expanded $EFPM_{2.5}$ of 35.3 g kg^{-1} for smoldering duff is much closer to our study best estimate. The FOFEM expanded $EFPM_{2.5}$ value for duff was derived from the literature synthesis of Urbanski (2014) and field measurements of peat fire emission measurements from Geron and Hays (2013) and specifically represents smoldering organic soil layers. Our study indicates FOFEM users concerned with $PM_{2.5}$ emissions from smoldering duff in Western conifer forests should employ the model's expanded $EFPM_{2.5}$. The use of the FOFEM default EF could lead to a large (approximately 50 percent) underprediction in $PM_{2.5}$ emissions from smoldering conifer duff.

In addition to $PM_{2.5}$, we have measured the EF for CO_2, CO, CH_4, and the sum of 19 NMHC. Carbon dioxide (CO_2) and CH_4 are both greenhouse gases, with CH_4 being approximately 28 times more potent than CO_2 (Myhre at al. 2013). The FOFEM default $EFCH_4$ is 13.8 g kg^{-1}, while the expanded FOFEM $EFCH_4$ is 7.9 g kg^{-1}. Our study's best estimate EFCH4 of 7.3 g kg^{-1} is in close agreement with the expanded FOFEM. For FOFEM users concerned with CH_4 emissions we recommend employing the expanded FOFEM EF to avoid a potentially large overestimation of CH_4 production.

Carbon monoxide (CO) can have both acute and long-term negative health effects. There are also grounds for concern that wildland firefighters can be exposed to potentially detrimental levels of CO while carrying out fireline duties (e.g. Semmens et al. 2021).

Our study's best estimate EFCO of 223 g kg^{-1} is lower than both the default and expanded FOFEM EFCO values of 302 g kg^{-1} and 257 g kg^{-1}, respectively. This comparison suggests a possible overprediction of CO emissions from smoldering duff, particularly when using the default FOFEM EF. None of the 19 NMHCs measured in our study is subject to NAAQS, and none are classified as hazardous air pollutants by the U.S. Environmental Protection Agency (USEPA 2023) and are unlikely to be of interest to land managers and not necessary for smoke management activities. However, our EFNMHC may be of interest to atmospheric chemists.

4. Conclusions

The purpose of this study is the improvement of emissions estimates for the management of smoke from prescribed fires. Our study focused on Douglas-fir duff for the following reasons: (1) the prominence of this forest type in western U.S., (2) the lack of EF measurements for smoldering conifer duff, and (3) the current and planned expansion of prescribed fire use in the West (see for example the USDA Forest Service Wildfire Crisis Strategy (WCS) Implementation Plan (USDA 2022)). We report the EF of $PM_{2.5}$, CO_2, CO, CH_4, and the sum of 19 NMHC measured for smoldering duff during laboratory burns of duff harvested from Douglas-fir forest stands. The study average EF (in units of g kg^{-1}) for CO_2, CO, CH_4, NMHC, and $PM_{2.5}$ were 1296 (1211, 1385), 223 (205, 239), 7.30 (4.07, 11.23), 10.08 (5.80, 15.04), 47.9 (14.6, 90.8), respectively, where the numbers in parentheses are 95 percent credible intervals based on the Bayesian framework analysis. Our study indicates that smoldering conifer duff $PM_{2.5}$ emissions calculated with the widely used land management model FOFEM may underestimate true $PM_{2.5}$ emissions by 25 percent to 50 percent. Such an underprediction in $PM_{2.5}$ emissions from smoldering duff could result in unexpected smoke impacts on communities and roadways near prescribed burns in conifer forests. If significant, local smoke impacts can result in obscuration of roadways with smoke, negative health effects on at-risk individuals, and potential violation of NAAQS and/or State and local regulations.

References

Abatzoglou, J.T.; Williams A.P. 2016. Impact of anthropogenic climate change on wildfire across western US forests. Proceedings of the National Academy of Sciences of the United States of America 113(42): 11770-11775. https://dx.doi.org/10.1073/pnas.1607171113

Agee, J.K.; Skinner, C.N. 2005. Basic principles of forest fuel reduction treatments. Forest Ecology and Management. 211(1-2): 83-96. https://dx.doi.org/10.1016/j.foreco.2005.01.034

Ager, A.A.; Day, M.A.; McHugh, C.W.; [et al.]. 2014. Wildfire exposure and fuel management on western US national forests. Journal of Environmental Management. 145: 54-70. https://dx.doi.org/10.1016/j.jenvman.2014.05.035

Akagi, S.K.; Yokelson, R.J.; Wiedinmyer, C.; [et al.]. 2011. Emission factors for open and domestic biomass burning for use in atmospheric models. Atmospheric Chemistry and Physics. 11(9): 4039-4072. https://dx.doi.org/10.5194/acp-11-4039-2011

Aphalo P. 2024. ggpmisc: Miscellaneous Extensions to 'ggplot2'. R package version 0.6.1, https://github.com/aphalo/ggpmisc, https://docs.r4photobiology.info/ggpmisc/

Alvarado, M.J.; Lonsdale, C.R.; Yokelson, R.J.; [et al.]. 2015. Investigating the links between ozone and organic aerosol chemistry in a biomass burning plume from a prescribed fire in California chaparral. Atmospheric Chemistry and Physics. 15(12): 6667-6688. https://dx.doi.org/10.5194/acp-15-6667-2015

Andreae, M.O. 2019. Emission of trace gases and aerosols from biomass burning—an updated assessment. Atmospheric Chemistry and Physics. 19(13): 8523-8546. https://dx.doi.org/10.5194/acp-19-8523-2019

Ashley, W.S.; Strader, S.; Dziubla, D.C.; [et al.]. 2015. Driving Blind: Weather-related vision hazards and fatal motor vehicle crashes. Bulletin of the American Meteorological Society. 96(5): 755-778. https://dx.doi.org/10.1175/BAMS-D-14-00026.1

ASTM International. 2014. ASTM D 2974-14 Standard test methods for moisture, ash, and organic matter of peat and other organic soils. ASTM International: West Conshohocken, PA. https://www.astm.org/d2974-20e01.html [Accessed 03 March 2024]

Bartolome, C.; Princevac, M.; Weise, D.R.; [et al.] 2019. Laboratory and numerical modeling of the formation of superfog from wildland fires. Fire Safety Journal. 106: 94-104. https://dx.doi.org/10.1016/j.firesaf.2019.04.009

Bertschi, I.; Yokelson, R. J; Ward, D.E.; [et al.] 2003. Trace gas and particle emissions from fires in large diameter and belowground biomass fuels. Journal of Geophysical Research-Atmospheres. 108(D13). https://dx.doi.org/10.1029/2002jd002100

Bhattarai, C.; Samburova, V.; Sengupta, D.; [et al.]. 2018. Physical and chemical characterization of aerosol in fresh and aged emissions from open combustion of biomass fuels. Aerosol Science and Technology. 52(11): 1266-1282. https://doi.org/10.1029/2002jd002100

Black, R.R.; Aurell, J.; Holder, A.; [et al.]. 2016. Characterization of gas and particle emissions from laboratory burns of peat. Atmospheric Environment 132: 49-57. https://dx.doi.org/10.1016/j.atmosenv.2016.02.024

Brey, S.J.; Ruminski, M.; Atwood, S.A. 2018. Connecting smoke plumes to sources using Hazard Mapping System (HMS) smoke and fire location data over North America. Atmospheric Chemistry and Physics. 18(3): 1745-1761. https://dx.doi.org/10.5194/acp-18-1745-2018

Buchholz, R.R.; Park, M.; Worden, H.M.; [et al.]. 2022. New seasonal pattern of pollution emerges from changing North American wildfires. Nature Communications. 13: 2043. https://doi.org/10.1038/s41467-022-29623-8

Burling, I.R.; Yokelson, R.J.; Akagi, S.K.; [et al.]. 2011. Airborne and ground-based measurements of the trace gases and particles emitted by prescribed fires in the United States. Atmospheric Chemistry and Physics. 11(23): 12197-12216. https://doi.org/10.5194/acp-11-12197-2011

Cancellieri, D.; Leroy-Cancellieri, V.; Leoni, E.; [et al.]. 2012. Kinetic investigation on the smouldering combustion of boreal peat. Fuel. 93: 479-485. https://dx.doi.org/10.1016/j.fuel.2011.09.052

Chakrabarty, R.K.; Gyawali, M.; Yatavelli, R.L.N.; [et al.]. 2016. Brown carbon aerosols from burning of boreal peatlands: Microphysical properties, emission factors, and implications for direct radiative forcing. Atmospheric Chemistry and Physics. 16(5): 3033-3040. https://dx.doi.org/10.5194/acp-16-3033-2016

Chen, H.; Zhao, W.;Liu, N.; [et al.]. 2013. Thermal decomposition extent of duff due to surface forest fire. Procedia Engineering. 62: 1000-1006. https://doi.org/10.1016/j.proeng.2013.08.154

Chen, H.; Zhao, W.; Liu, N.; 2011. Thermal analysis and decomposition kinetics of Chinese forest peat under nitrogen and air atmospheres. Energy & Fuels. 25(2): 797-803. https://dx.doi.org/10.1021/ef101155n

Childs, M.L.; Li, J.S.C.; Wen, J.F.; 2022. Daily local-level estimates of ambient wildfire smoke PM2.5 for the contiguous US. Environmental Science & Technology. 56: 13607–13621. https://doi.org/10.1021/acs.est.2c02934

Christian, T.J.; Kleiss, B.; Yokelson, R.J.; [et al.]. 2003. Comprehensive laboratory measurements of biomass-burning emissions: 1. Emissions from Indonesian, African, and other fuels. Journal of Geophysical Research-Atmospheres. 108 (D23): 4719. https://dx.doi.org/10.1029/2003jd003704

Cowan, D.A.; Page, W.G.; Butler, B.W.; [et al.]. 2020. Effects of fuel characteristics on horizontal spread rate and ground surface temperatures of smouldering duff. International Journal of Wildland Fire. 29(9): 820-831. https://dx.doi.org/10.1071/WF19207

David, L.M.; Ravishankara, A.R.; Brey, S.J.; [et al.]. 2021. Could the exception become the rule? 'Uncontrollable' air pollution events in the US due to wildland fires. Environmental Research Letters. 16(3): 034029. https://dx.doi.org/10.1088/1748-9326/abe1f3

Frandsen, W.H. 1997. Ignition probability of organic soils. Canadian Journal of Forest Research. 27: 1471–1477. https://dx.doi.org/10.1139/x97-106

Frandsen, W.H. 1987. The influence of moisture and mineral soil on the combustion limits of smoldering forest duff. Canadian Journal of Forest Research. 17: 1540–1544. https://dx.doi.org/10.1139/x87-236

Freeborn, P.H.; Wooster, M.J.; Hao, W.M.; [et al.]. 2008. Relationships between energy release, fuel mass loss, and trace gas and aerosol emissions during laboratory biomass fires. Journal of Geophysical Research-Atmospheres. 113: D01301. https://dx.doi.org/10.1029/2007JD008679

Gelman, A.; Rubin, D. B. 1992. Inference from iterative simulation using multiple sequences. Statistical Science. 7(4): 457–472. http://www.jstor.org/stable/2246093

Geron, C.; Hays, M. 2013. Air emissions from organic soil burning on the coastal plain of North Carolina. Atmospheric Environment. 64: 192-199. https://dx.doi.org/10.1016/j.atmosenv.2012.09.065

Grulke, N.E.; Heath, R.L. 2020. Ozone effects on plants in natural ecosystems. Plant Biology. 22:12-37. https://dx.doi.org/10.1111/plb.12971

Holden, Z.A.; Swanson, A.; Luce, C.H.; [et al.]. 2018. Decreasing fire season precipitation increased recent western US forest wildfire activity. Proceedings of the National Academy of Sciences of the United States of America. 115(36): E8349-E8357. https://dx.doi.org/10.1073/pnas.1802316115

Horel, J.; Splitt, M.; Dunn, L.; [et al.]. 2002. Mesowest: Cooperative mesonets in the western United States. Bulletin of the American Meteorological Society. 83(2): 211-226. https://doi.org/10.1175/1520-0477(2002)083%3C0211:MCMITW%3E2.3.CO;2

Hu, Y.Q.; Christensen, E.; Restuccia, F.; [et al.]. 2019. Transient gas and particle emissions from smouldering combustion of peat. Proceedings of the Combustion Institute. 37(3): 4035-4042. https://dx.doi.org/10.1016/j.proci.2018.06.008

Huang, X.; Rein, G. 2016. Thermochemical conversion of biomass in smouldering combustion across scales: The roles of heterogeneous kinetics, oxygen and transport phenomena. Bioresource Technology. 207: 409-421. https://dx.doi.org/10.1016/j.biortech.2016.01.027

Jaffe, D.A.; O'Neill, S.M.; Larkin, N.K.; [et al.]. 2020. Wildfire and prescribed burning impacts on air quality in the United States. Journal of the Air & Waste Management Association. 70: 583-615. https://dx.doi.org/10.1080/10962247.2020.1749731

Jaffe, D.A.; Wigder, N.L. 2012. Ozone production from wildfires: A critical review. Atmospheric Environment. 51: 1–10. https://dx.doi.org/10.1016/j.atmosenv.2011.11.063

Jayarathne, T.; Stockwell, C.E.; Gilbert, A.A.; [et al.]. 2018. Chemical characterization of fine particulate matter emitted by peat fires in Central Kalimantan, Indonesia, during the 2015 El Nino. Atmospheric Chemistry and Physics. 18: 2585-2600. https://dx.doi.org/10.5194/acp-18-2585-2018

Jen, C.N.; Hatch, L.E.; Selimovic, V.; [et al.]. 2019. Speciated and total emission factors of particulate organics from burning western US wildland fuels and their dependence on combustion efficiency. Atmospheric Chemistry and Physics. 19: 1013-1026. https://dx.doi.org/10.5194/acp-19-1013-2019

Kassambara, A. 2023. ggpubr: 'ggplot2' Based Publication Ready Plots. R package version 0.6.0. https://rpkgs.datanovia.com/ggpubr/

Kitzberger, T.; Brown, P.M.; Heyerdahl, E.K.; [et al.]. 2007. Contingent Pacific-Atlantic Ocean influence on multicentury wildfire synchrony over western North America. Proceedings of the National Academy of Sciences of the United States of America. 104: 543-548. https://dx.doi.org/10.1073/pnas.0606078104

Kuwata, M.; Neelam-Naganathan, G.G.; Miyakawa, T. 2018. Constraining the emission of particulate matter from Indonesian peatland burning using continuous observation data. Journal of Geophysical Research-Atmospheres. 123: 9828-9842. https://dx.doi.org/10.1029/2018JD028564

Lindaas, J.; Farmer, D.K.; Pollack, I.B.; [et al.]. 2017. Changes in ozone and precursors during two aged wildfire smoke events in the Colorado Front Range in summer 2015. Atmospheric Chemistry and Physics. 17: 10691-10707. https://dx.doi.org/10.5194/acp-17-10691-2017

Littell, J.S.; McKenzie, D.; Peterson, D.L.; [et al.]. 2009. Climate and wildfire area burned in western U.S. ecoprovinces, 1916-2003. Ecological Applications. 19: 1003-1021. https://doi.org/10.1890/07-1183.1

Liu, Y; Heilman, W.E.; Potter, B.E.; [et al.]. 2022. Smoke plume dynamics. In: Peterson, D.L.; McCaffrey, S.M.; Patel-Weynand, T.; eds. 2022. Wildland fire smoke in the United States: A scientific assessment. Cham, Switzerland: Springer Nature Switzerland AG. 83–119. https://doi.org/10.1007/978-3-030-87045-4_4

Lopez, G.; Basterra, L.A.; Acuna, L.; [et al.]. 2013. Determination of the emissivity of wood for inspection by infrared thermography. Journal of Nondestructive Evaluation. 32: 172-176. https://dx.doi.org/10.1007/s10921-013-0170-3

Lutes, D.C. 2020. FOFEM 6.7: First order fire effects model user guide. U.S. Department of Agriculture, Forest Service, Rocky Mountain Research Station, Fire Modeling Institute. 92 p. http://firelab.org/project/fofem

McClure, C.D.; Jaffe, D.A. 2018. US particulate matter air quality improves except in wildfire-prone areas. Proceedings of the National Academy of Sciences of the United States of America. 115: 7901-7906. https://dx.doi.org/10.1073/pnas.1804353115

Melvin, M.A. 2018. National prescribed fire use survey report. Technical Report 03-18. Coalition of Prescribed Fire Councils, Inc. 23 p. http://www.prescribedfire.net/ [Accessed 2024 November 4]

Miller, C.; O'Neill, S.; Rorig, M; [et al.]. 2019. Air-quality challenges of prescribed fire in the complex terrain and wildland urban interface surrounding Bend, Oregon. Atmosphere. 10: 515. https://dx.doi.org/10.3390/atmos10090515

Mitchell, D.; Smidt, M. 2019. Costs of mechanical fuel reduction treatments. In: Manzello, S. eds. Encyclopedia of wildfires and wildland-urban interface (WUI) fires. Springer, Cham. 7p. https://doi.org/10.1007/978-3-319-51727-8_139-1

Myhre, G.; Shindell, D.; Bréon, F.–M.; 2013. Anthropogenic and natural radiative forcing. In Climate change 2013: The physical science basis. Contribution of Working Group I to the Fifth Assessment Report of the Intergovernmental Panel on Climate Change. Stocker, T.F.; Qin, D.; Plattner, G.-K.; [et al.] eds. Cambridge, U.K: Cambridge University Press. 659-740. https://doi.org/10.1017/CBO9781107415324.018

National Wildfire Coordinating Group. 2020a. Smoke and roadway safety guide. Boise, ID: National Wildfire Coordinating Group. 47 p. PMS 477. https://www.nwcg.gov/publications/pms477 [Accessed 2024 November 04]

National Wildfire Coordinating Group. 2020b. NWCG smoke management guide for prescribed fire. Boise, ID: National Wildfire Coordinating Group. PMS 420-3. 297 p. https://www.nwcg.gov/publications/pms420-3 [Accessed 2024 November 04]

Nolan R.; Padilla-Parra, S. 2018. ijtiff: An R package providing TIFF I/O for ImageJ users. Journal of Open Source Software. 3(23): 633. 10.21105/joss.00633. https://doi.org/10.21105/joss.00633

O'Dell, K.; Ford, B.; Fischer, E.V.; [et al.]. 2019. Contribution of wildland-fire smoke to US PM2.5 and its influence on recent trends. Environmental Science & Technology. 53: 1797-1804. https://dx.doi.org/10.1021/acs.est.8b05430

Ottmar, R.D. 2014. Wildland fire emissions, carbon, and climate: Modeling fuel consumption. Forest Ecology and Management. 317: 41-50. https://dx.doi.org/10.1016/j.foreco.2013.06.010

Palamba, P.; Werdhani, A.S.; Numberi, J.J. 2023. Smoldering behavior of peat fire. IOP Conference Series: Earth and Environmental Science. 1192 012039. https://doi.org/10.1088/1755-1315/1192/1/012039 [3 March 2025]

Prichard, S.J.; O'Neill, S.M.; Eagle, P. 2020. Wildland fire emission factors in North America: Synthesis of existing data, measurement needs and management applications. International Journal of Wildland Fire. 29: 132-147. https://dx.doi.org/10.1071/WF19066

Prichard, S.J; Rowell, E.M.; Hudak, A. [et al.]. 2022. Chapter 2. Fuels and consumption. In: Peterson, David L.; McCaffrey, Sarah M.; Patel-Weynand, Toral, eds. 2022. Wildland fire smoke in the United States: A scientific assessment. Cham, Switzerland: Springer Nature Switzerland AG. p. 11-49. https://doi.org/10.1007/978-3-030-87045-4_2

R Core Team. 2023. R: A language and environment for statistical computing. Vienna, Austria: R Foundation for Statistical Computing. https://www.R-project.org/

Reid, C.E.; Brauer, M.; Johnston, F.H.; [et al.]. 2016. Critical review of health impacts of wildfire smoke exposure. Environmental Health Perspectives. 124: 1334-1343. https://dx.doi.org/10.1289/ehp.1409277

Rein, G. 2016. Smoldering combustion. In: Hurley, M.J.; [et al.], eds. SFPE Handbook of fire protection engineering. New York: Springer. https://doi.org/10.1007/978-1-4939-2565-0_19

Roulston, C.; Paton-Walsh, C.; Smith, T.E.L.; [et al.]. 2018. Fine particle emissions from tropical peat fires decrease rapidly with time since ignition. Journal of Geophysical Research-Atmospheres. 123: 5607-5617. https://dx.doi.org/10.1029/2017JD027827

Ruefenacht, B.; Finco, M.V.; Nelson, M.D.; [et al.]. 2008. Conterminous US and Alaska forest type mapping using Forest Inventory and Analysis data. Photogrammetric Engineering and Remote Sensing. 74: 1379-1388. https://doi.org/10.14358/PERS.74.11.1379

Selimovic, V.; Yokelson, R.J.; Warneke, C.; [et al.]. 2018. Aerosol optical properties and trace gas emissions by PAX and OP-FTIR for laboratory-simulated western US wildfires during FIREX. Atmospheric Chemistry and Physics. 18: 2929-2948. https://dx.doi.org/10.5194/acp-18-2929-2018

Semmens, E.O.; Leary, C.S.; West, M.R.; [et al]. 2021. Carbon monoxide exposures in wildland firefighters in the United States and targets for exposure reduction. Journal of Exposure Science & Environmental Epidemiology. 31: 923–929. https://doi.org/10.1038/s41370-021-00371-z

Signorell A.; Aho K.; Alfons A.; [et al.]. 2023. DescTools: tools for descriptive statistics. R package version 09945. https://cran.r-project.org/web/packages/DescTools/index.html

Soil Survey Staff. 2022. Keys to Soil Taxonomy, 13th ed. USDA Natural Resources Conservation Service. https://www.nrcs.usda.gov/sites/default/files/2022-09/Keys-to-Soil-Taxonomy.pdf

Stephens, S.L.; Battaglia, M.A.; Churchill, D.J.; [et al.]. 2021. Forest restoration and fuels reduction: Convergent or divergent? Bioscience. 71: 85-101. https://dx.doi.org/10.1093/biosci/biaa134

Stockwell, C.E.; Jayarathne, T.; Cochrane, M.A.; [et al.]. 2016. Field measurements of trace gases and aerosols emitted by peat fires in Central Kalimantan, Indonesia, during the 2015 El Nino. Atmospheric Chemistry and Physics. 16: 11711-11732. https://dx.doi.org/10.5194/acp-16-11711-2016

Stockwell, C.E.; Yokelson, R.J.; Kreidenweis, S.M.; [et al.]. 2014. Trace gas emissions from combustion of peat, crop residue, domestic biofuels, grasses, and other fuels: Configuration and Fourier transform infrared (FTIR) component of the fourth Fire Lab at Missoula Experiment (FLAME-4). Atmospheric Chemistry and Physics. 14: 9727-9754. https://dx.doi.org/10.5194/acp-14-9727-2014

Urbanski, S. 2014. Wildland fire emissions, carbon, and climate: Emission factors. Forest Ecology and Management. 317: 51-60. https://dx.doi.org/10.1016/j.foreco.2013.05.045

Urbanski, S.P.; O'Neill, S.M.; Holder, A.L.; [et al.]. 2022. Chapter 5. Emissions. In: Peterson, David L.; McCaffrey, Sarah M.; Patel-Weynand, Toral, eds. Wildland fire smoke in the United States: A scientific assessment. Cham, Switzerland: Springer Nature Switzerland AG: 121-165. https://doi.org/10.1007/978-3-030-87045-4_5

Urbanski, S.P.; Reeves, M.C.; Corley, R.E.; [et al.]. 2018. Contiguous United States wildland fire emission estimates during 2003-2015. Earth System Science Data. 10: 2241-2274. https://dx.doi.org/10.5194/essd-10-2241-2018

U.S. Department of Agriculture [USDA]. 2022. Confronting the wildfire crisis: 10-year implementation plan. FS-1187-b. Washington, DC: U.S. Department of Agriculture, Forest Service. 14 p. https://www.fs.usda.gov/sites/default/files/Wildfire-Crisis-Implementation-Plan.pdf

U.S. Department of Agriculture [USDA]. 2014. United States forest resource facts and historical trends. FS-1035. Washington, DC: U.S. Department of Agriculture, Forest Service. 64 p. https://www.fia.fs.fed.us/library/brochures/docs/2012/ForestFacts_1952-2012_English.pdf

U.S. Environmental Protection Agency [USEPA]. 2023. Initial list of hazardous air pollutants with modifications. Washington, DC: U.S. Environmental Protection Agency. https://www.epa.gov/haps/initial-list-hazardous-air-pollutants-modifications#mods [February 1, 2023]

U.S. Environmental Protection Agency [USEPA]. 2022. Other Test Method 48 (OTM-48): Emission factor determination by the carbon balance method. Washington, DC: U.S. Environmental Protection Agency. https://www.epa.gov/emc/emc-other-test-methods

U.S. Environmental Protection Agency [USEPA]. 2021a. Comparative assessment of the impacts of prescribed fire versus wildfire (CAIF): A case study in the western U.S. EPA/600/R-21/044. Washington, DC: U.S. Environmental Protection Agency. 146 p. https://cfpub.epa.gov/ncea/risk/recordisplay.cfm?deid=352824

U.S. Environmental Protection Agency [USEPA]. 2021b. 2017 National emissions inventory, January 2021 Sector summaries–Criteria and hazardous air pollutants by 60 EIS emission sectors. https://www.epa.gov/air-emissions-inventories/2017-national-emissions-inventory-nei-data

U.S. Environmental Protection Agency [USEPA]. 2020. Integrated science assessment (ISA) for ozone and related photochemical oxidants (Final Report, Apr 2020). EPA/600/R-20/012. Washington, DC: U.S. Environmental Protection Agency. https://cfpub.epa.gov/ncea/isa/recordisplay.cfm?deid=348522

U.S. Environmental Protection Agency [USEPA]. 2019. Integrated science assessment (ISA) for particulate matter (Final Report, Dec 2019). EPA/600/R-19/188. U.S. Environmental Protection Agency, Washington, DC. 1,967 p. https://cfpub.epa.gov/ncea/isa/recordisplay.cfm?deid=347534

U.S. Environmental Protection Agency [USEPA]. 1999. Determination of volatile organic compounds (VOCS) in ambient air using specially prepared canisters with subsequent analysis by gas chromatography. Compendium method TO-14A. EPA/625/R-96/010b. Washington, DC: U.S. Environmental Protection Agency. 90 p. https://www.epa.gov/sites/default/files/2019-11/documents/to-14ar.pdf

Usup, A.; Hashimoto, Y.; Takahashi, H.; [et al.]. 2004. Combustion and thermal characteristics of peat fire in tropical peatland in Central Kalimantan, Indonesia. Tropics. 14: 1-19. https://dx.doi.org/10.3759/tropics.14.1

Ward, D.E.; Hardy, C.C. 1989. Emissions from burning of chaparral. In: Proceedings. 1989 National Air and Waste Management Association meeting; 1989 June 25-30. Anaheim, CA: Air and Waste Management Association. https://www.frames.gov/documents/smoke/serdp/ward_hardy_1989b.pdf [Accessed 2024 November 04]

Ward, D.E.; Radke, L.F. 1993. Emissions measurements from vegetation fires: A comparative evaluation of methods and results. In: Crutzen, P.J. and Goldammer, J.G., eds. Fire in the environment: The ecological, atmospheric, and climatic importance of vegetation fires. New York: John Wiley & Sons: 53-76.

Ward D.E.; Hardy, C.C; Sandberg. D.; [et al.]. 1989. Mitigation of prescribed fire atmospheric pollution through increased utilization of hardwoods, piled residues, and long-needled conifers. Part III—Emission characterization. Final report to the Bonneville Power and U.S. Department of Energy under IAG-DE-AI179-85BP18509. Portland, OR: U.S. Department of Energy, Northwest Research Station. 110 p.

Watson, J.G.; Cao, J.; Chen, L.W.A.; [et al.]. 2019. Gaseous, PM2.5 mass, and speciated emission factors from laboratory chamber peat combustion. Atmospheric Chemistry and Physics. 19: 14173-14193. https://dx.doi.org/10.5194/acp-19-14173-2019

Westerling, A.L. 2016. Increasing western US forest wildfire activity: Sensitivity to changes in the timing of spring. Philosophical Transactions of the Royal Society B-Biological Sciences. 371:20150178. https://dx.doi.org/10.1098/rstb.2015.0178

Wickham H. 2011. The split-apply-combine strategy for data analysis. Journal of Statistical Software. 40(1): 1–29. https://doi.org/10.18637/jss.v040.i01

Wickham H. 2016. ggplot2: Elegant graphics for data analysis. New York: Springer-Verlag. https://doi.org/10.1007/978-3-319-24277-4

Wittig, V.E.; Ainsworth, E.A.; Naidu, S.L.; [et al.]. 2009. Quantifying the impact of current and future tropospheric ozone on tree biomass, growth, physiology and biochemistry: A quantitative meta-analysis. Global Change Biology. 15: 396-424. https://dx.doi.org/10.1111/j.1365-2486.2008.01774.x

Wooster, M.J.; Gaveau, D.L.A.; Salim, M.A.; [et al.]. 2018. New tropical peatland gas and particulate emissions factors indicate 2015 Indonesian fires released far more particulate matter (but less methane) than current inventories imply. Remote Sensing. 10: 495. https://dx.doi.org/10.3390/rs10040495

Wooster, M.J.; Roberts, G.; Perry, G.L.W.; [et al.]. 2005. Retrieval of biomass combustion rates and totals from fire radiative power observations: FRP derivation and calibration relationships between biomass consumption and fire radiative energy release. Journal of Geophysical Research-Atmospheres. 110: 1-24. https://dx.doi.org/10.1029/2005JD006318

Yang, J.; Chen, H.; Zhao, W.; [et al.]. 2016. Combustion kinetics and emission characteristics of peat by using TG-FTIR technique. Journal of Thermal Analysis and Calorimetry. 124: 519-528. https://dx.doi.org/10.1007/s10973-015-5168-x

Yokelson, R.J.; Saharjo, B.H.; Stockwell, C.E.; [et al.]. 2022. Tropical peat fire emissions: 2019 field measurements in Sumatra and Borneo and synthesis with previous studies. Atmospheric Chemistry and Physics 22:10173-10194. https://dx.doi.org/10.5194/acp-22-10173-2022

Yokelson, R.J.; Burling, I.R.; Gilman, J.B.; [et al.]. 2013. Coupling field and laboratory measurements to estimate the emission factors of identified and unidentified trace gases for prescribed fires. Atmospheric Chemistry and Physics. 13: 89-116. https://dx.doi.org/10.5194/acp-13-89-2013

Yokelson, R.J.; Goode, J.G.; Ward, D.E.; [et al.]. 1999. Emissions of formaldehyde, acetic acid, methanol, and other trace gases from biomass fires in North Carolina measured by airborne Fourier transform infrared spectroscopy. Journal of Geophysical Research-Atmospheres. 104: 30109-30125. https://dx.doi.org/10.1029/1999JD900817

Youngflesh, C. 2018. MCMCvis: Tools to visualize, manipulate, and summarize MCMC output. Journal of Open Source Software, 3(24): 640. https://dx.doi.org/10.21105/joss.00640

Zhao, W.; Chen, H.; Liu, N.; [et al.]. 2014. Thermogravimetric analysis of peat decomposition under different oxygen concentrations. Journal of Thermal Analysis and Calorimetry. 117: 489-497. https://dx.doi.org/10.1007/s10973-014-3696-4

Zhu, H; Liu, N. 2020. Thermal decomposition of biomass and shallow soil mixtures. Fire Safety Journal. 113: 102990. https://dx.doi.org/10.1016/j.firesaf.2020.102990

Appendix A—Blackbody Calibration of Infrared Camera

The FLIR SC6700 infrared camera used in this study measured photon counts, which were converted to temperatures utilizing a blackbody calibration performed previously (Cowan et al. 2020). In our study, the calibration used blackbody temperatures that ranged from 100 °C to 550 °C and an integration time of 4.96 ms. The blackbody calibration—blackbody temperature (T_C_BB) as a function of blackbody intensity (I_BB)—is shown in figure A.1. The blackbody temperatures determined from the calibration, T_C_BB, were converted to duff surface temperature, T_{sfc} (C), using equation A1:

$$T_{sfc} = \left(\frac{\varepsilon_{BB} T_K\_BB}{\varepsilon_{sfc}} \right) - 273.15 \quad \text{(A.1)}$$

where

T_{sfc} = duff surface temperature (C),

ε_{BB} = 0.98, the emissivity from the blackbody calibration,

T_K_BB = blackbody temperature (K),

ε_{sfc} = 0.85, the emissivity of the duff surface based on values measured for heated wood (Lopez et al. 2013).

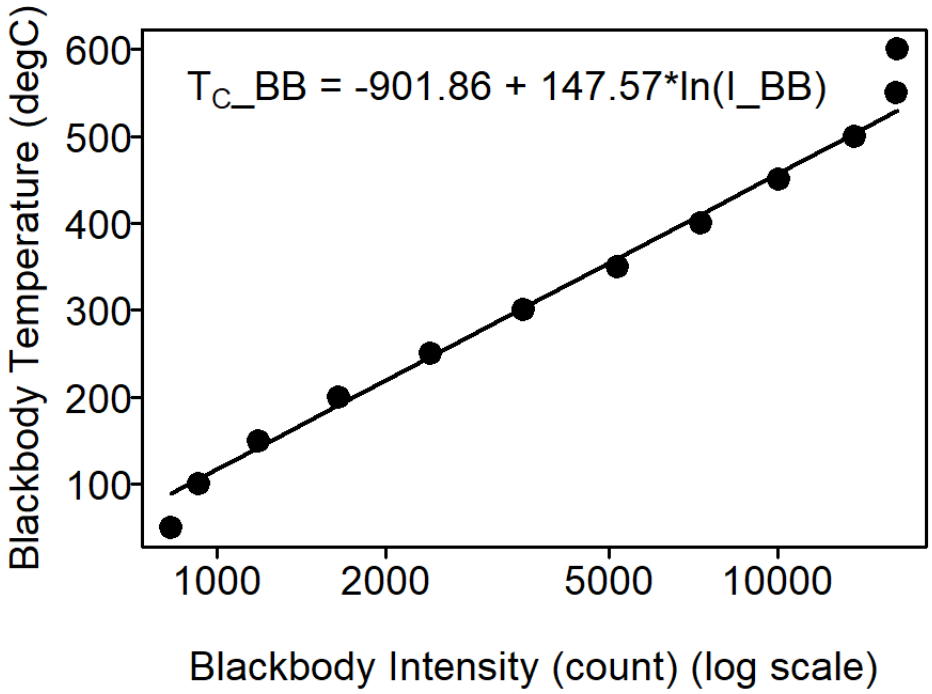

Figure A.1—Blackbody temperature (T_C_BB; C) plotted versus the natural log of blackbody intensity (I_BB; photon count) with best fit least-squares linear regression model. Calibration valid over range of 926 counts (100 °C) to 13696 counts (500 °C).

Appendix B—Images of the Emission Sampling Apparatus

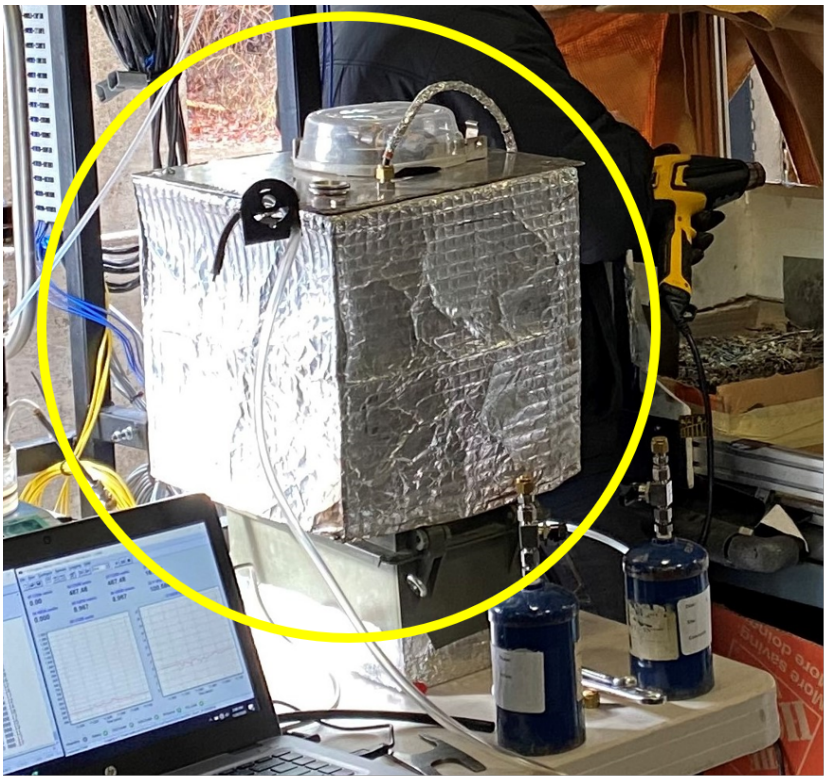

Figure B.1—Emissions sampling chamber

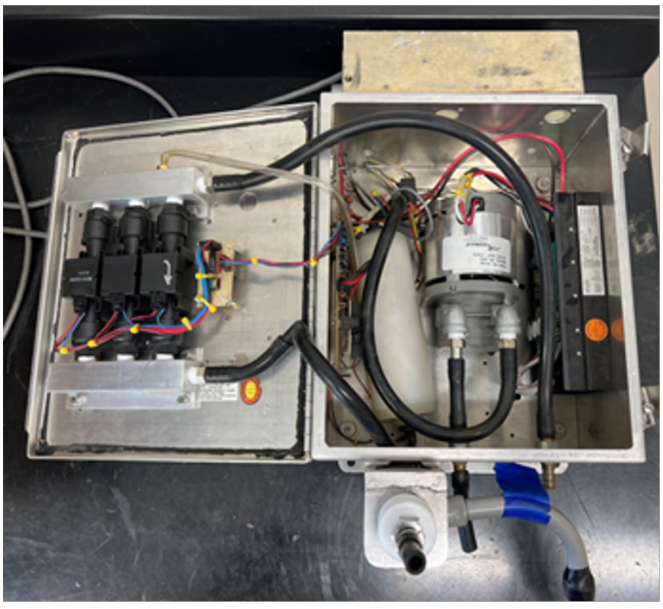

Figure B.2—Filter sampling system

Appendix C—List of NMHC

List C.1—Names and formulas of the 19 nonmethane hydrocarbons measured.

Ethane (C_2H_6)
Ethene (C_2H_4)
Ethyne (C_2H_2)
Propane (C_3H_8)
Propene (C_3H_6)
Propyne (C_3H_4)
Butane (C_4H_{10})
trans-2-Butene (C_4H_8)
Butene (C_4H_8)
iso-Butene ($C_4H_{8)}$
cis-2-Butene (C_4H_8)
1,3-Butadiene (C_4H_6)
iso-Pentane (C_5H_{12})
Pentane (C_5H_{12})
cis- or trans-Pentene (C_5H_{10})
1-Pentene (C_5H_{10})
cis- or trans-Pentene (C_5H_{10})
Hexane (C_6H_{14})
Hexene (C_6H_{14})

Appendix D—Emission Factors from January 2020 Burns

Table D.1—Burn average EF (g kg^{-1}) from January 2020 testing. Values in parenthesis are one standard deviation. These data are being included for completeness. Due to the peculiar combustion behavior of the January burns and the possibility ambient conditions were not representative of broadcast prescribed burns in the western U.S., this data should not be used for estimating emissions (see Section 3.1).

Data field	Burn 1	Burn 2	Burn 3	Burn 4
Date	28-Jan-2020	29-Jan-2020	30-Jan-2020	31-Jan-2020
Number of samples	6	9	6	15
MCE	0.833 (0.017)	0.847 (0.022)	0.863 (0.025)	0.824 (0.009)
Carbon dioxide (CO_2)	886.9 (47.2)	1163.8 (153.9)	1043.9 (34.5)	1268.6 (24.2)
Carbon monoxide (CO)	112.9 (8.9)	132.2 (12.0)	105.6 (19.0)	172.3 (8.8)
Methane (CH_4)	5.45 (1.56)	7.13 (1.33)	3.38 (0.87)	3.44 (0.48)
NMHC	5.03 (1.24)	7.45 (1.84)	2.98 (1.27)	5.20 (0.92)
$PM_{2.5}$	22.0 (14.6)	72.8 (58.1)	NM	16.0 (7.1)

Appendix E—Plots of Bayesian Model Results

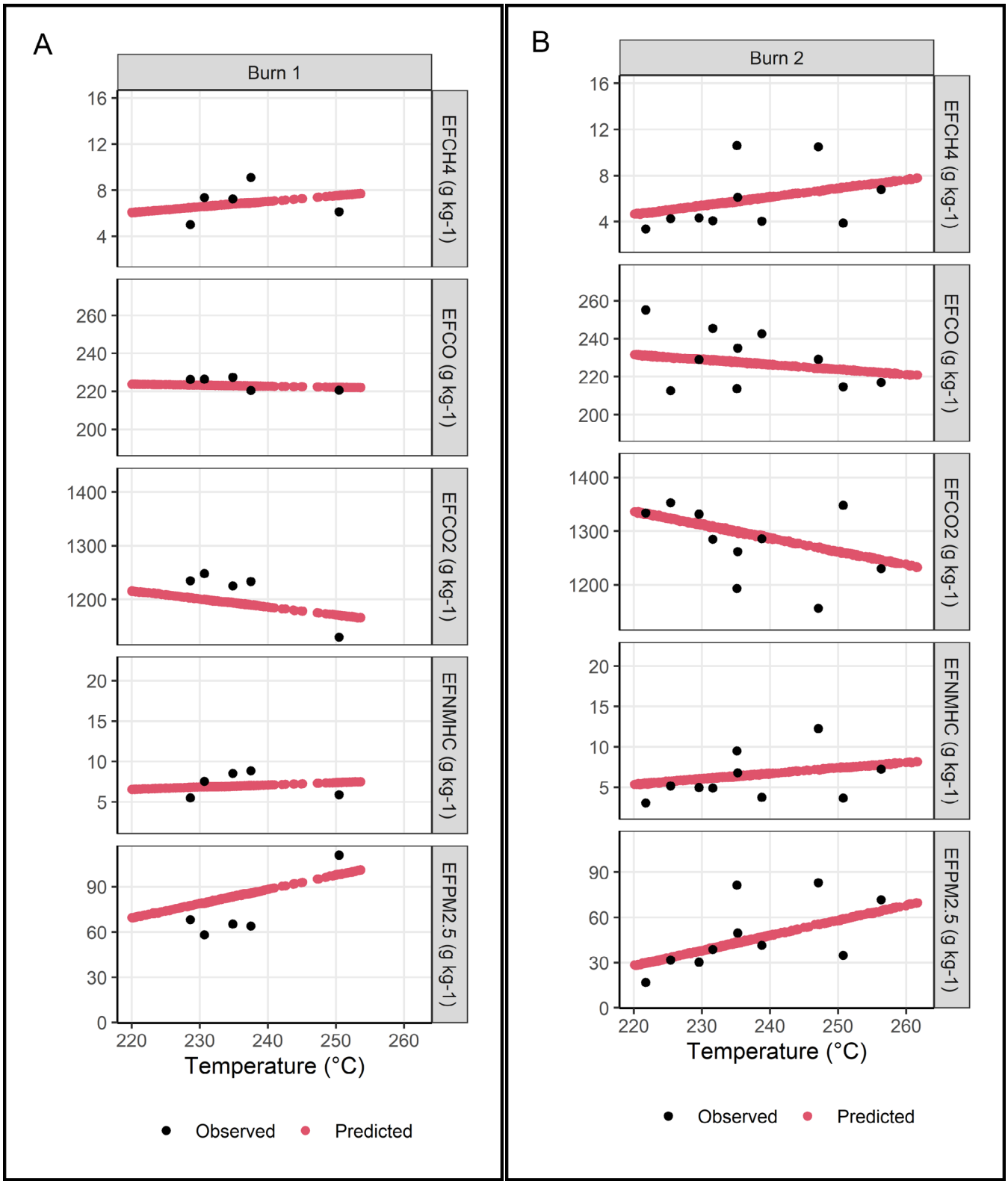

Figure E.1A—The EF (g kg^{-1}) plotted versus T (°C) for burns 1-2 (A-B). Black markers are the observed The EF and pink markers are the posterior means (EF predicted by Bayesian model) for each observation in the imputed time series.

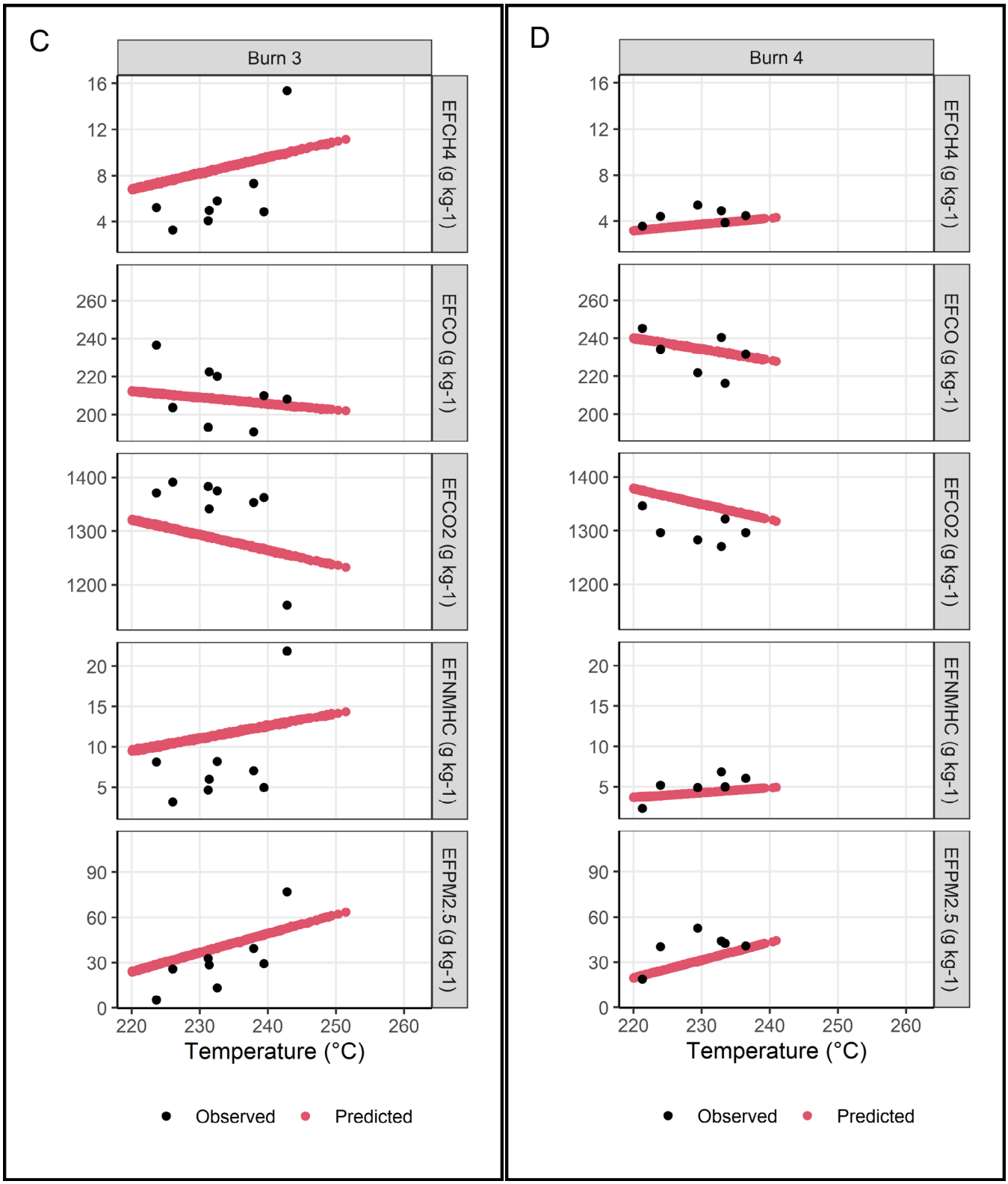

Figure E.1B—The EF (g kg^{-1}) plotted versus T (°C) for burns 3-4 (C-D). Black markers are the observed The EF and pink markers are the posterior means (EF predicted by Bayesian model) for each observation in the imputed time series.

To learn more about RMRS publications or search our online titles:

https://research.fs.usda.gov/rmrs/products/publications

https://research.fs.usda.gov/treesearch